Mid-Miocene paleoproductivity in the Atlantic Ocean and implications for the global carbon cycle

Liselotte Diester-Haass,[1] Katharina Billups,[2] Darren R. Gröcke,[3] Louis François,[4] Vincent Lefebvre,[5] and Kay C. Emeis[6]

Received 5 February 2008; revised 6 August 2008; accepted 20 November 2008; published 18 February 2009.

[1] A prominent, middle Miocene (17.5–13.5 Ma) carbon isotope excursion ubiquitously recorded in carbonate sediments has been attributed to enhanced marine productivity and sequestration of ^{13}C depleted organic carbon in marine sediments or enhanced carbon burial in peat/lignite deposits on land. Here we test the hypothesis that the marine $\delta^{13}C$ record reflects a change in productivity with proxy records from three Atlantic Ocean sites (Deep Sea Drilling Program Site 608 and Ocean Drilling Program Sites 925 and 1265). Our multiproxy approach is based on benthic foraminiferal accumulation rates, elemental ratios (Ba/Al and P/Al), the $\delta^{13}C$ of bulk sedimentary organic matter, and dissolution indices. We compare these proxies to benthic foraminiferal $\delta^{13}C$ values measured on the same samples. Our results indicate that marine paleoproductivity in the Atlantic Ocean is not related to the benthic foraminiferal $\delta^{13}C$ excursion. A numerical box model confirms that marine productivity cannot account for the $\delta^{13}C$ maximum. The model shows that sequestration of 1.5×10^{18} mol C in the terrestrial realm over a period of 3 Ma leads to a 0.9‰ $\delta^{13}C$ increase in the deep ocean, which is near the observed records. Therefore, an increase in continental organic carbon sequestration is the most plausible way to enrich the ocean's carbon pool with ^{13}C, which is consistent with coeval lignite deposits worldwide. The $\delta^{13}C$ values of bulk sedimentary organic matter parallel the $\delta^{13}C$ of dissolved inorganic carbon as reflected by benthic foraminiferal $\delta^{13}C$ values suggesting no significant change in atmospheric pCO_2 levels over the investigated period.

Citation: Diester-Haass, L., K. Billups, D. R. Gröcke, L. François, V. Lefebvre, and K. C. Emeis (2009), Mid-Miocene paleoproductivity in the Atlantic Ocean and implications for the global carbon cycle, *Paleoceanography*, *24*, PA1209, doi:10.1029/2008PA001605.

1. Introduction

[2] The late early through middle Miocene saw important changes in the climate system both in the marine and terrestrial realm The warmest interval of the Neogene, the so-called ''middle Miocene climatic optimum'' [*Savin et al.*, 1985; *Woodruff and Savin*, 1985] occurred at 17 Ma. Vegetation is thought to have extended to high latitudes with evergreen forests proliferating to 45°N in North America and 52°N in Europe [*Utescher et al.*, 2000]. Major deposits of brown coal are found worldwide [*Utescher et al.*, 2000; *Föllmi et al.*, 2005; *Holdgate et al.*, 2007]. This interval of time is accompanied by an increase in $\delta^{13}C$ values of foraminifera, which, appropriately, has been termed the ''middle Miocene $\delta^{13}C$ shift'' [*Savin et al.*, 1985; *Woodruff and Savin*, 1985].

[3] The warmest interval of the Neogene at 17 Ma was followed by rapid cooling and growth of Antarctic ice sheets at ~14 Ma [e.g., *Flower and Kennett*, 1993; *Zachos et al.*, 2001; *Holbourn et al.*, 2004]. The degree of global cooling is evidenced by benthic oxygen isotope and Mg/Ca records [*Savin et al.*, 1985; *Woodruff and Savin*, 1985; *Billups and Schrag*, 2002; *Shevenell et al.*, 2004], which point to a dramatic (~5–8°C) temperature drop at ~14 Ma, ice volume increase, and rapid sea level changes [*Flower and Kennett*, 1994; *Miller et al.*, 1991; *Browning et al.*, 2006]. Global cooling at ~14 Ma has been cited as the driver of increased continental aridity and expansion of C_4 grasslands [*Retallack*, 2001; *Jia et al.*, 2003], which replaced the dense, warm-adapted flora dominating the earlier Miocene. Furthermore, brown coal deposition ceased during this interval of time [*Utescher et al.*, 2000]. Deep-sea $\delta^{13}C$ values decreased and returned to preexcursion values about 1 million years later by ~13 Ma.

[4] Superimposed on the positive $\delta^{13}C$ excursion are six distinct carbon isotope maxima termed ''CM events'' by *Woodruff and Savin* [1989, 1991]. Because CM events are recorded in benthic and planktic foraminiferal $\delta^{13}C$ records from all ocean basins, they are deemed global features that are important for mid-Miocene isotope stratigraphy [e.g., *Loutit*, 1981; *Keigwin and Shackleton*, 1980; *Vincent et al.*,

[1]Zentrum für Umweltwissenschaften, Universität des Saarlandes, Saarbrücken, Germany.
[2]College of Marine and Earth Studies, University of Delaware, Lewes, Delaware, USA.
[3]Department of Earth Sciences, Durham University, Durham, UK.
[4]Institut d'Astrophysique et de Géophysique, Université de Liège, Liège, Belgium.
[5]UMR Géosystèmes, UFR des Sciences de la Terre, Université des Sciences et Technologies de Lille, Villeneuve d'Ascq, France.
[6]Institut für Biogeochemie und Meereschemie, Universität Hamburg, Hamburg, Germany.

0883-8305/09/2008PA001605$12.00

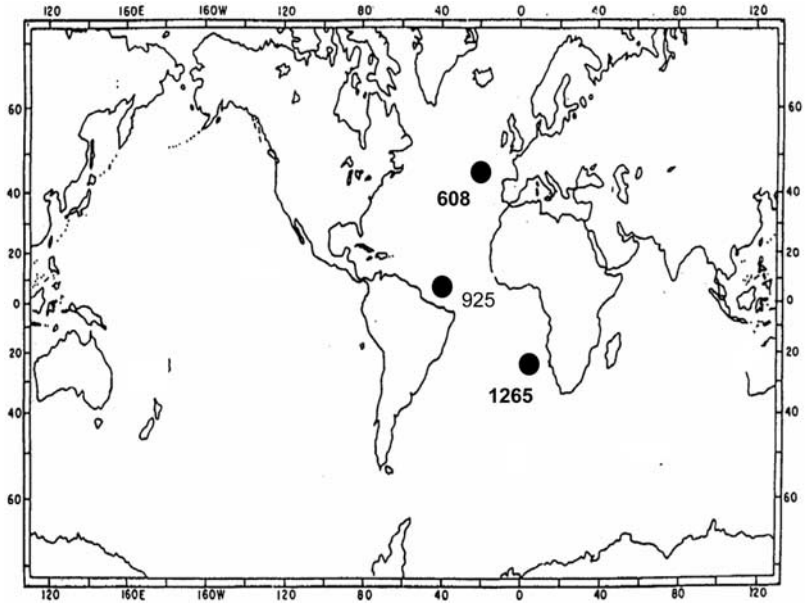

Figure 1. Location of investigated ODP sites in the Atlantic Ocean. Table 1 contains information on water depth and present-day productivity.

1980; *Keigwin*, 1987; *Woodruff and Savin*, 1991; *Flower and Kennett*, 1993].

[5] *Vincent and Berger* [1985] proposed that high $\delta^{13}C$ values during the mid-Miocene reflect enhanced carbon sequestration in organic-rich sediments along the circum-Pacific margins, an idea termed the "Monterey Hypothesis." According to this hypothesis, the burial of organic carbon in nascent upwelling environments resulted in the drawdown of atmospheric CO_2 levels that caused subsequent global cooling and the expansion of ice on Antarctica at ~14 Ma. Proxy-based reconstructions and modeling suggest an increase in net organic carbon flux from the oceanic to the sedimentary reservoir during the mid-Miocene until ~14 Ma [*Southam and Hay*, 1981; *Derry and France-Lanord*, 1996]. Sediments from the Caribbean (e.g., increase in mass accumulation rates of pelagic carbonate; phosphogenesis [*Mutti et al.*, 2005]), Florida continental margin (phosphogenesis [*Compton et al.*, 1990]), Mediterranean Sea (phosphogenesis [*Jacobs et al.*, 1996; *Föllmi et al.*, 2008]) and circum-Pacific margin (diatomaceous shales with very high organic matter content [*Vincent and Berger*, 1985]) also point to enhanced primary productivity. *Woodruff and Savin* [1985] were the first to propose that relatively high foraminiferal $\delta^{13}C$ values in the Miocene are, at least in part, associated with higher open ocean productivity and carbon burial in the Pacific Ocean.

[6] However, the "Monterey Hypothesis" cannot explain the time lag between the onset of the positive carbon isotope excursion at ~17.5 Ma, and global cooling at ~14 Ma, even if individual organic rich deposits within the Monterey Formation correlate with times of increased deep sea cooling and positive $\delta^{13}C$ values [e.g., *Flower and Kennett*, 1993]. Also, recent calculations suggest that the amount of organic carbon embedded in the Monterey Formation may not be sufficient to impact global climate [*Isaacs*, 2001; *John et al.*, 2002; *Föllmi et al.*, 2005]. Furthermore, atmospheric CO_2 levels remain relatively constant and low throughout the Miocene [*Spivack et al.*, 1993; *Pagani et al.*, 1999, 2000; *Demicco et al.*, 2003]. Therefore Antarctic ice sheet expansion at ~14 Ma may not be related to atmospheric CO_2 drawdown, but rather to changes in surface ocean circulation [e.g., *Shevenell et al.*, 2004] and/or intervals of prolonged low Southern Hemisphere insolation [*Holbourn et al.*, 2005].

[7] Here we investigate whether or not, or the extent to which, mid-Miocene $\delta^{13}C$ records can be related to changes in primary marine productivity. To address this issue we have constructed productivity records based on benthic foraminiferal accumulation rates from three sites in the Atlantic Ocean (Figure 1). The records span the late-early Miocene through late mid-Miocene (~19–11 Ma). The sites are from regions outside of upwelling areas dominated by carbonate sedimentation. In support of the foraminifer-derived paleoproductivity reconstructions we assess barium and phosphorus content, as well as calcium carbonate accumulation rates in order to monitor surface water carbonate productivity [e.g., *Murray and Peterson*, 1997; *Ravelo et al.*, 1997; *Grant and Dickens*, 2002]. We use dissolution proxy records (percent sand size fraction, percent test fragmentation of planktonic foraminifera, and benthic/planktonic foraminiferal test ratios) to constrain the effects of corrosive bottom waters on the sedimentary record. We also constructed benthic foraminiferal $\delta^{13}C$ records at each site in order to be able to directly compare the productivity records to $\delta^{13}C$ variations measured in the same samples. We have measured the $\delta^{13}C$ values of bulk sedimentary organic matter at all three sites in order to investigate possible relationships between productivity, carbonate $\delta^{13}C$, relative changes in atmospheric CO_2 levels and terrestrial input. Last, we use a box model to test which

Table 1. Summary of Site Locations

Site	Water Depth (m)	Latitude	Longitude	Modern Productivity (gC cm^{-2} ka^{-1})
608	3526[a]	42°50.205′N	23°05.252′W	15[b]
925	3042	4°12.249′N	43°29.3′E	15[b]
1265	3060	28°50.10′S	02°38.35′E	10[b]

[a]Paleodepth 3100–3400 m [*Wright et al.*, 1992].
[b]*Antoine et al.* [1996].

aspect of the carbon cycle can best explain the proxy based observations.

2. Approach

2.1. Site Locations

[8] We chose Deep Sea Drilling Project Site 608 in the North Atlantic and two Ocean Drilling Program sites (Sites 925 and 1265) located in the northwestern tropical and southeastern subtropical Atlantic, respectively (Figure 1 and Table 1). Site 608 is situated on the southern flank of King's Trough and lies within the northern part of the modern subtropical gyre [*Ruddiman et al.*, 1987]. Site 925 is located on Ceara Rise in the western equatorial Atlantic Ocean [*Curry et al.*, 1995]. Modern day surface hydrography here is characterized by a seasonally deep mixed layer, convergence and downwelling [*Peterson and Stramma*, 1991]. Site 1265 is positioned on the northern flank of Walvis Ridge in the subtropical South Atlantic toward the western reaches of the northward flowing Benguela Current [*Shipboard Scientific Party*, 2004]. At all three sites, modern day primary productivity is relatively low with values of between 10 and 15 g C cm^{-2} ka^{-1} [*Antoine et al.*, 1996] (Table 1).

2.2. Stratigraphy and Mass Accumulation Rates

[9] Mid-Miocene sedimentary sequences typically contain unconformities and dissolution events [*Keller and Barron*, 1983; *Woodruff and Savin*, 1991] that compromise continuity of proxy records. Accordingly, at Site 608, there is a hiatus causing a gap between ~14.2 Ma and 13.8 Ma. At Site 925, this period of time is marked by a minimum in linear sedimentation rates. Additionally, while Site 925 has an otherwise complete and multiple cored Miocene sedimentary record, proxy records from Sites 608 and 1265 contain gaps at core breaks.

[10] Among the three sites, Site 925 has the most precise age control because it is based on tuning physical parameters to astrochronology (H. Pälike, personal communication, 2006). For Site 608 and 1265 we rely on shipboard biostratigraphic datums (*Ruddiman et al.* [1987] and *Shipboard Scientific Party* [2004], respectively) and revisions to these provided in recent studies involving these sites [*Wright et al.*, 1992, *Pagani et al.*, 1999]. Finally, we have updated the ages to the recent time scale of *Gradstein et al.* [2004], which is based on orbitally tuned control points. Thus, the age models at the three sites are comparable, at least at the level of the temporal resolution of our study (20–50 ka).

[11] Mass accumulation rates (MAR) are commonly used to assess temporal changes in the individual sediment components such as $CaCO_3$, or benthic foraminifera. MARs, however, are not truly independent measures of sediment accumulation because of their dependence on linear sedimentation rates (LSR). Therefore, the validity of MARs and thus the derived productivity proxies depends on age control. To calculate MARs, we linearly interpolated between age control points to derive LSR (cm ka^{-1}) and multiplied them with the dry bulk density (g cm^{-3}). MAR is expressed as gram dry sediment accumulating per cm^{-2} per ka (g cm^{-2} ka^{-1}).

2.3. Paleoproductivity From Benthic Foraminifera

[12] Benthic foraminiferal accumulation rates (BFAR) have been used extensively as a proxy for paleoproductivity [*Herguera and Berger*, 1991; *Nees*, 1997; *Schmiedl and Mackensen*, 1997; *Yasuda*, 1997; *van der Zwaan et al.*, 1999; *Diester-Haass et al.*, 2004, 2005, 2006; *Diester-Haass and Nees*, 2004, *Holbourn et al.*, 2005]. *Diester-Haass et al.* [2005] review the derivation of paleoproductivity estimates in g C cm^{-2} ka^{-1} from foraminiferal accumulation rates based on the work of *Herguera* [2000]

$$PP = 0.4Z^{*}BFAR^{0.5} \quad (1)$$

where PP stands for paleoproductivity and is related to the flux of organic carbon to the seafloor (g C cm^{-2} ka^{-1}), Z is the water depth, and BFAR is the benthic foraminiferal accumulation rate (tests cm^{-2} ka^{-1}) derived by multiplying the test counts per gram sediment with the MAR.

[13] As discussed by *Diester-Haass et al.* [2005], this approach assumes a constant relationship between surface water organic matter production and export production on the one hand, and export production and the amount of organic carbon reaching the sediments on the other hand [e.g., *Herguera*, 2000]. Furthermore, MAR-based studies, such as the BFAR approach, are dependent on the age model. Hence, it is important to apply a multiproxy approach that also involves other records of surface water productivity that are independent of sediment accumulation rates such as elemental ratios.

2.4. Carbonate Accumulation and Preservation

[14] Changes in $CaCO_3$ MAR (obtained by multiplying the MAR by the fraction of $CaCO_3$) can be used to assess changes in surface water productivity if carbonate dissolution is negligible. Because coccoliths constitute the bulk of inorganic carbon at our sites $CaCO_3$-MARs provide a measure primarily of coccolithophorid productivity [e.g., *Berger et al.*, 1993; *Siesser*, 1995; *Grant and Dickens*, 2002; *Diester-Haass et al.*, 2005, 2006].

[15] Dissolution limits the extent to which $CaCO_3$ accumulation can be used as a proxy for surface water productivity, and it also limits the extent to which the accumulation of geochemical sediment components reflects surface water productivity [e.g., *Anderson and Winckler*, 2005]. Benthic to planktonic foraminiferal test ratios (B/P) or the percent sand-sized fraction of the sediments can be used as dissolution proxies as well as a fragmentation index based on the ratio between fragmented planktonic foraminiferal tests and the total amount of planktonic foraminiferal tests (whole

and fragments) in a sample [e.g., *Keigwin*, 1976; *Dittert et al.*, 1999; *Diester-Haass et al.*, 2005, 2006].

2.5. The $\delta^{13}C$ Values of Bulk Sedimentary Organic Matter

[16] We have measured the $\delta^{13}C$ values of bulk sedimentary organic matter ($\delta^{13}C_{org}$) at all three sites in order to investigate possible relationships between productivity, carbonate $\delta^{13}C$, relative changes in atmospheric CO_2 levels and terrestrial input. Comparisons between $\delta^{13}C_{org}$ and $\delta^{13}C_{carb}$ can be used as a qualitative measure of the CO_2 in surface waters [e.g., *Hayes et al.*, 1989; *Rau et al.*, 1989, 1997; *Jasper and Hayes*, 1994; *Francois et al.*, 1993]. Although this proxy does not provide absolute estimates, it offers a relative measure of pCO_2 (increase or decrease) that can be directly compared against more precise paleoestimates, such as alkenones [*Pagani et al.*, 1999, 2000]. We then use the difference between the $\delta^{13}C$ values of the benthic foraminifera, which we take to reflect the $\delta^{13}C$ of dissolved inorganic carbon, and the bulk $\delta^{13}C_{org}$ value of sedimentary organic matter as an indicator of carbon isotope fractionation and thus atmospheric pCO_2 [*Rau et al.*, 1997].

2.6. Elemental Ratios as Paleoproductivity Proxies

[17] Independent evidence for changes in productivity comes from ratios of barium and phosphorus as "biogenic" to aluminum or titanium as "detrital" elements. Numerous studies have used this approach to assess changes in paleoproductivity in the Pleistocene [*Averyt and Paytan*, 2004], and Miocene [e.g., *Weedon and Shackleton*, 1997; *Grant and Dickens*, 2002]. Ba/Al ratios in excess of those in regional detrital inputs are often used for qualitative [*Schmitz*, 1987] or quantitative reconstructions of the organic carbon export of the seafloor [e.g., *Francois et al.*, 1995; *Dymond et al.*, 1992; *Eagle et al.*, 2003; *Reitz et al.*, 2004]. The approach hinges on assumptions related to the source of excess Ba being marine biogenic barite and the regional detrital Ba/Al (or Ba/Ti) background ratio being known and relatively constant through time [*Averyt and Paytan*, 2004; *Anderson and Winckler*, 2005].

[18] Another commonly used productivity indicator is the ratio of P/Al. It provides information on the availability of P from continental weathering, or the decoupling of P availability from weathering fluxes because of changes in ocean circulation and chemistry [e.g., *Delaney and Boyle*, 1987; *Filippelli and Delaney*, 1995; *Filippelli*, 1997]. Again, this approach assumes that the flux of Al (or Ti) remained constant through time.

2.7. Numerical Box Modeling

[19] To explore the magnitudes of changes in marine and terrestrial carbon pools and their isotope ratios in the global carbon cycle to be expected from the middle Miocene isotope shift, we adapted a numerical box model to permit sensitivity studies. *Isaacs* [2001] and *Föllmi et al.* [2005] have shown that the ~1‰ $\delta^{13}C$ excursion cannot be explained entirely by an increase in marine organic carbon burial from circum-Pacific Monterey type sediments. Here we use a box model of the global carbon cycle to evaluate the effect of terrestrial carbon burial on the global carbon cycle and the oceanic $\delta^{13}C$ signature. These sensitivity tests were conducted with a model updated from the version of *Grard et al.* [2005]; details are provided in Appendix A.

3. Analytical Methods

[20] Samples (20 cm^3) were split for geochemical and micropaleontological analyses. For sedimentological-micropaleontological studies 10 cm^3 were oven-dried at 60°C, weighed, washed through 40 and 63 μm sieves, dried and dry sieved into subfractions (63–125, 125–250, 250–500, >500 μm). In each fraction 800 grains (if present) were counted and various biogenic, clastic and authigenic components differentiated to yield percentage composition of the sand fraction. The numbers of benthic foraminifera in the three fractions were summed up and divided by the weight of the total analyzed sample to give the number of benthic foraminifera per gram of total sediment.

[21] Carbon isotope analyses were conducted on 1–5 *Cibicidoides wuellerstorfi* and *C. mundulus* picked from the > 255 μm fraction. At Sites 608 and 1265 we note a small (0.2‰) difference between the $\delta^{13}C$ values of *C. wuellerstorfi* and *C. mundulus*. We subtract 0.2‰ from the *C. wuellerstorfi* $\delta^{13}C$ values to bring them in line with *C. mundulus*, which dominate the downcore records. All samples were sonicated in deionized water to remove adhering sediment and oven-dried for at least 24 h prior to isotopic analysis. Analyses were performed at the University of Delaware using a GVI IsoPrime equipped with a Multiprep peripheral for the automated reaction of individual samples with phosphoric acid (at 90°C). Using NBS-19 and an in-house standard (Carrara Marble) the precision for $\delta^{13}C$ and $\delta^{18}O$ values is better than 0.05‰ and 0.08‰, respectively, in the size range of the samples (20–200 μg).

[22] Stable isotope analysis of bulk sedimentary organic matter was performed on decarbonated samples. One cm^3 of the sample was placed in a 50 ml centrifuge tube and reacted with 3 mol L^{-1} HCl overnight. Because of the relatively high amount of carbonate in these sediments, fresh HCl was added the following day and if no effervescence occurred the samples were rinsed until neutrality was obtained. No samples reacted after the overnight treatment. Samples were then oven-dried at 60°C for at least 24 h prior to isotopic analysis. Analyses were performed at McMaster University using a Thermo-Finnigan DeltaPlus XP equipped with a Costech elemental analyzer for combustion of the sediment samples. Up to 8 international and internal standards were analyzed during the generation of these isotopic data and precision of $\delta^{13}C_{org}$ was 0.1‰. Because of the low concentration of organic matter within these sediments, isotopic analysis was performed without dilution and sample sizes ranged between 1.2 to 1.5 mg in order to produce an intensity >1000 mV. Analytical reproducibility of replicate samples was on average 0.2‰.

[23] Total inorganic carbon (TIC) and major element composition were determined on the other half of the bulk sediments after freeze drying and grinding in an agate mortar. Total carbon was determined on all samples by combustion at 1200°C and detection with a thermal conductivity detector (NA 1500 Carlo Erba). TIC was determined coulometrically after acidification of weighed sample

splits with 1N HCl in a Juwe Coulomat 702 instrument. Concentrations of aluminum, phosphorus and barium were analyzed on fused (600 mg of sample diluted with 3600 mg of lithium tetraborate) discs in an automated X-ray fluorescence spectrometer MagixPRO (Panalytical) that is equipped with a Rh anode. Loss on ignition was determined at 110°C and at 1000°C. Concentrations of major and trace elements were calculated on the basis of a calibration against international standards. Ratios of Ba/Al and P/Al were calculated as weight ratios of the elements barium, aluminum, and phosphorus in the samples.

4. Results

4.1. Site 608

[24] The mid-Miocene $\delta^{13}C$ shift is well expressed in the North Atlantic benthic foraminiferal $\delta^{13}C$ values, which begin to increase at ~17.5 Ma, remain high until 13.5 Ma, and decrease thereafter (Figure 2a). We recognize several well-defined smaller $\delta^{13}C$ maxima superimposed on the long-term trend (Figure 2a). These individual $\delta^{13}C$ maxima (~15.7 Ma, 15.2 Ma, 14.7 Ma, and 13.5 Ma) correspond to CM 3, CM 4, CM 5, and CM 6, which are generally recognized in Miocene marine sections [*Woodruff and Savin*, 1991] providing a check on the comparability of the age models among the sites.

[25] Benthic foraminiferal $\delta^{18}O$ values are relatively low until ~14.4 Ma, increase between 14.4 Ma and 13.4 Ma, and remain high thereafter (Figure 2b). A hiatus leaves a ~0.4 Ma gap in the record (14.2–13.8 Ma) so that the $\delta^{18}O$ maximum outlining the major step in ice volume increase as Antarctic ice sheets expand during the mid-Miocene is not present (Figure 2b). The beginning of increasing $\delta^{18}O$ values at 14.4 Ma predates the timing of the increase seen in orbitally tuned records where it occurs at ~14.0–13.9 Ma [*Holbourn et al.*, 2005]. At this scale, the discrepancy likely reflects uncertainties associated with relatively coarsely spaced biostratigraphic age control points.

[26] There is little agreement in the long-term trends among the proxy records that would suggest a relationship between productivity and the foraminiferal $\delta^{13}C$ records. There is no apparent association between the mid-Miocene $\delta^{13}C$ maximum and productivity. BFAR derived paleoproductivity increases gradually from 18 Ma to 12 Ma (Figure 2c), a trend is also seen in the $CaCO_3$ MAR (Figure 2i) and that may be linked to an overall increase in LSR (Figure 2k). The $\delta^{13}C_{org}$ record (Figure 2d) displays a trend toward increasing values beginning at ~17.5 Ma, remains relatively high until ~13.8 Ma, after which point it decreases toward a minimum at ~13.3 Ma. Thus, the overall character of this trend is similar to the benthic foraminiferal $\delta^{13}C$ record (Figure 2a). The similarity of these carbon isotope records is highlighted by their difference ($\Delta^{13}C$, Figure 2e), which remains relatively constant over the long term.

[27] Linear sedimentation rates (Figure 2k), as well as $CaCO_3$ accumulation (Figure 2i) increase gradually from 18 to 12 Ma and the long-term trend in the paleoproductivity record may at least in part reflect the overall increase in MARs. The percent $CaCO_3$ (Figure 2j), a measure that is independent of age control, shows a parallel increase suggesting that the overall increase in sediment accumulation may have been brought about by relatively enhanced carbonate deposition/preservation. There are no marked changes in the long-term trend of the dissolution indices (B/P ratio and % fragmentation), but the timing of smaller-scale variations agrees well (Figures 2f and 2g, respectively).

4.2. Site 925

[28] In the tropical Atlantic, benthic foraminiferal $\delta^{13}C$ values also display the well-defined mid-Miocene $\delta^{13}C$ maximum (Figure 3a). Two individual $\delta^{13}C$ maxima clearly stand out above the background, and the timing agrees with the timing of CM 5 at 14.7 Ma and CM 6 at 13.5 Ma as observed at Site 608 (Figure 2a). The interval corresponding to CM 3 (15.8 Ma) is characterized by generally high $\delta^{13}C$ values and the excursion is not well defined, possibly because of a gap in the $\delta^{13}C$ record just preceding the event. CM 4 is absent and $\delta^{13}C$ values remain constant until decreasing just prior to CM 5.

[29] Benthic foraminiferal $\delta^{18}O$ values follow the global middle Miocene pattern with relatively low values until ~14 Ma, a rapid increase between 14.0 Ma and 13.8 Ma, and relatively high values thereafter (Figure 3b). The rapid $\delta^{18}O$ increase between 14.0 and 13.8 Ma is entirely consistent with other orbitally tuned $\delta^{18}O$ records [*Holbourn et al.*, 2005].

[30] As shown at Site 608, the paleoproductivity and benthic foraminiferal $\delta^{13}C$ records do not show any similarity over the long term (Figure 3c). Paleoproductivity fluctuated about a constant mean until 14.4 Ma, where it displays a pronounced minimum between 14.4 Ma and 13.8 Ma and increases thereafter, a pattern tracking the LSR (Figure 3k).

[31] The long-term component of the $\delta^{13}C_{org}$ values does not follow the benthic foraminiferal $\delta^{13}C$ values as observed at Site 608 (Figure 3d). Instead, the $\delta^{13}C_{org}$ curve fluctuates widely about a long-term mean of approximately −24‰ before ~15 Ma, and at approximately −22‰ after 13.5 Ma. Because foraminiferal $\delta^{13}C$ values decrease after 13.5 Ma, while the $\delta^{13}C_{org}$ values increase, the $\Delta^{13}C$ curve shows a pronounced (4‰) increase between 13.5 and 12.5 Ma (Figure 3e). This would be consistent with a change in pCO_2, but is, perhaps more likely, due to the vicinity of the Amazon River [*Hoorn et al.*, 1995] and the type of organic matter preserved.

[32] Linear sedimentation rates decrease slightly between 18 and 11 Ma, but there are relatively large variations. For example, a prolonged maximum is centered at 15 Ma and an extreme minimum occurs between 14.4 and 13.8 Ma (Figure 3k). These maxima and minima transmit into the MAR derived records ($CaCO_3$ accumulation, Figure 3i and paleoproductivity, Figure 3c). $CaCO_3$ decreases by about 30% between 14.8 and 13.8 Ma (Figure 3j). Dissolution indices (Figures 3f and 3g) do not show any change during this portion of the record suggesting increasingly less carbonate production across the interval of major Antarctic ice expansion.

4.3. Site 1265

[33] In the southeastern subtropical Atlantic, benthic foraminiferal $\delta^{13}C$ values display the overall middle Miocene $\delta^{13}C$ maximum, but individual CM events are not readily apparent (Figure 4a). Although there is a core

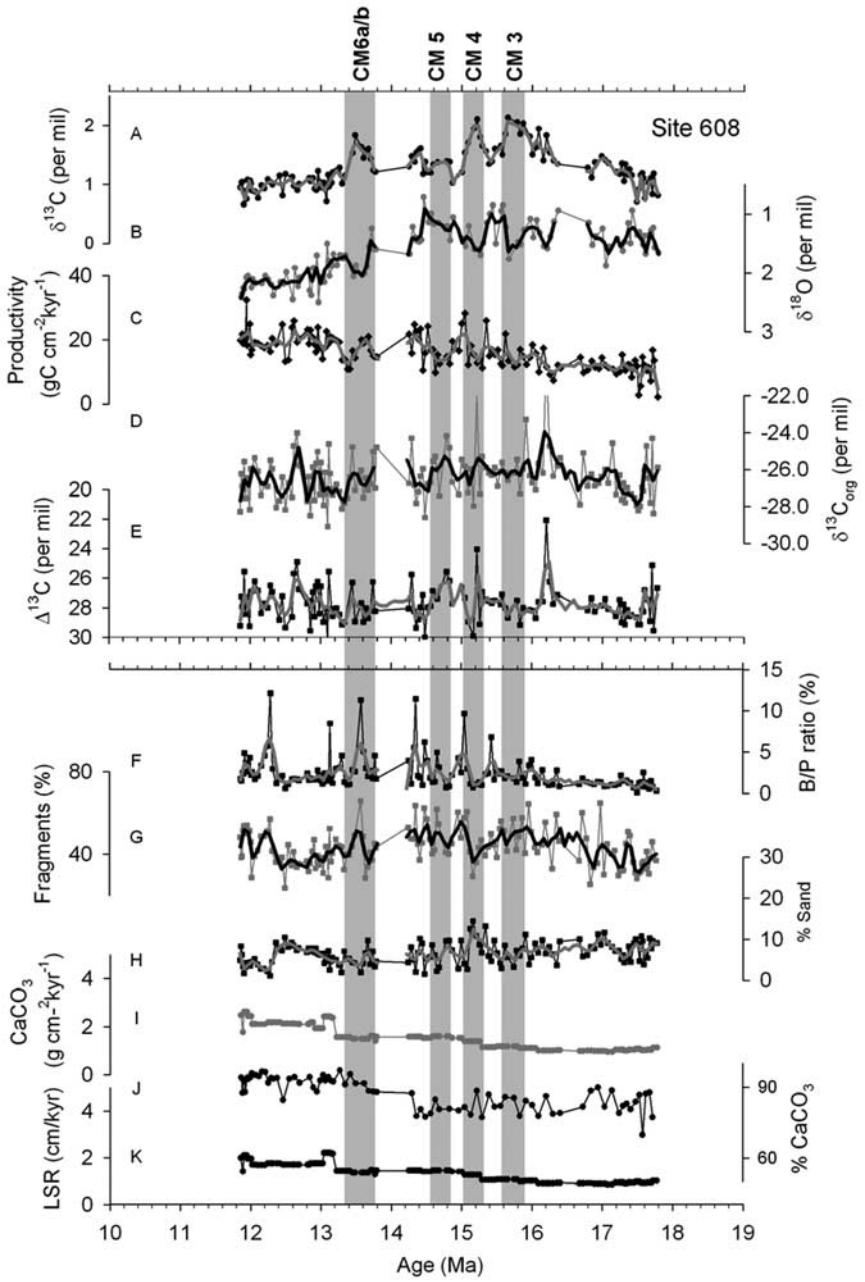

Figure 2. Results from North Atlantic Site 608. (a) Benthic foraminiferal $\delta^{13}C$ values, (b) benthic foraminiferal $\delta^{18}O$ values, (c) benthic foraminiferal mass accumulation rate derived paleoproductivity, (d) $\delta^{13}C$ of bulk sedimentary organic matter ($\delta^{13}C_{org}$), (e) the difference between foraminiferal $\delta^{13}C$ values and $\delta^{13}C_{org}$, (f) percent benthic to planktonic (B/P) foraminferal test ratio, (g) percent fragments, (h) percent sand (>63 μm) fraction of the sediments, (i) $CaCO_3$ mass accumulation, (j) percent $CaCO_3$, and (k) linear sedimentation rates (LSR). Vertical gray bars highlight the position of Miocene carbon isotope (CM) events [*Woodruff and Savin*, 1991]. Heavy lines in Figures 2a–2h reflect a Gaussian smoothing function with a 3% sampling portion.

break spanning the interval that would contain CM 3, the $\delta^{13}C$ values are constant between 15.4 (~CM 4) and 14.6 Ma (~CM 5), decrease rapidly until 14.0 Ma, and display a minor maximum at 13.2 Ma, and again at 12.6 Ma.

[34] The long-term trend in the $\delta^{18}O$ record mirrors the $\delta^{13}C$ record with a long minimum between 17 Ma and 14 Ma when $\delta^{13}C$ values are high. The $\delta^{18}O$ values decrease rapidly between 14.2 Ma and 14.0 Ma, suggesting that the ages may be ~0.2 Ma too old. For example, shifting

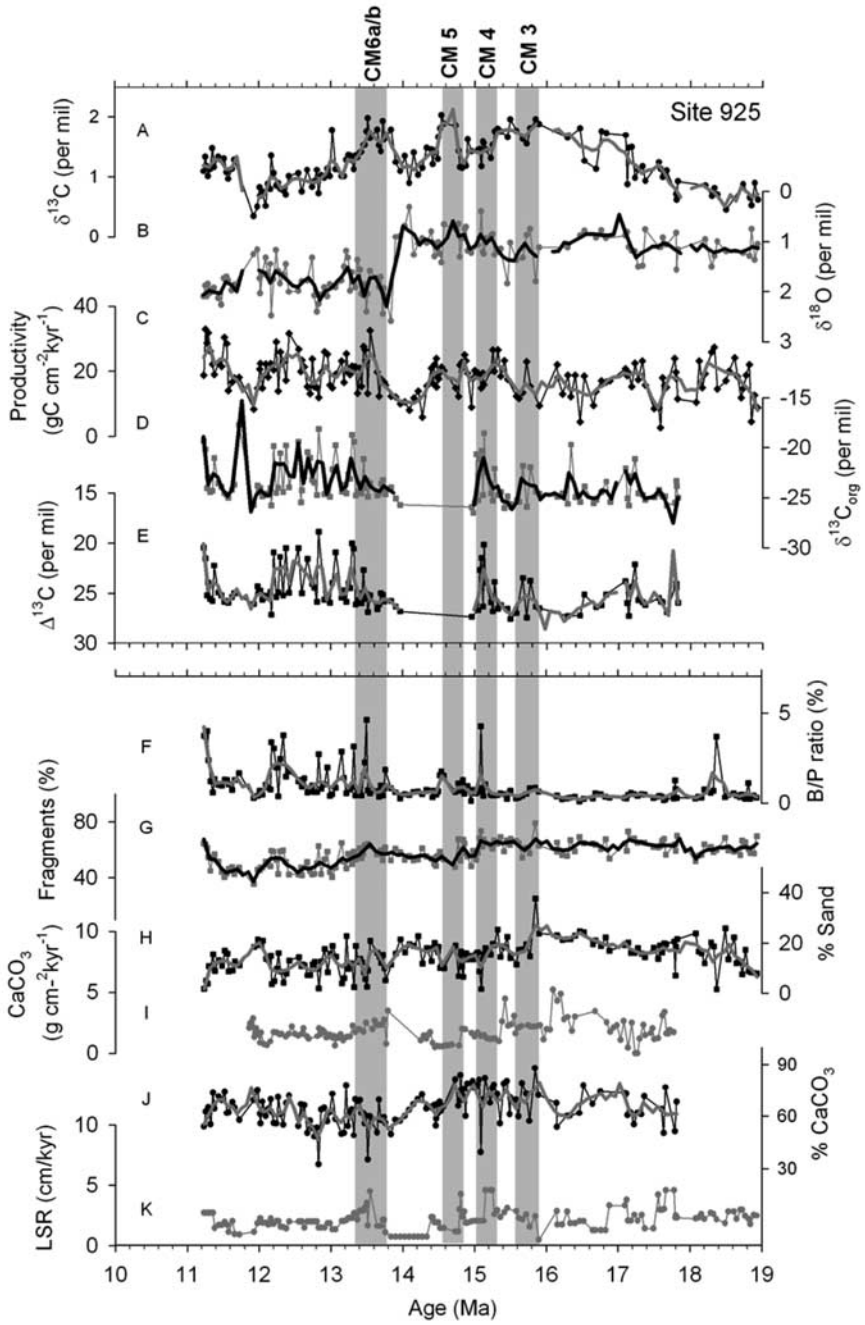

Figure 3. Results from tropical Atlantic Site 925. (a) Benthic foraminiferal $\delta^{13}C$ values, (b) benthic foraminiferal $\delta^{18}O$ values, (c) benthic foraminiferal mass accumulation rate derived paleoproductivity, (d) $\delta^{13}C$ of bulk sedimentary organic matter ($\delta^{13}C_{org}$), (e) the difference between foraminiferal $\delta^{13}C$ values and $\delta^{13}C_{org}$, (f) percent benthic to planktonic (B/P) foraminferal test ratio, (g) percent fragments, (h) percent sand (>63 μm) fraction of the sediments, (i) $CaCO_3$ mass accumulation, (j) percent $CaCO_3$, and (k) linear sedimentation rates (LSR). Vertical gray bars highlight the position of Miocene carbon isotope (CM) events [*Woodruff and Savin*, 1991]. Heavy lines in Figures 3a–3h reflect a Gaussian smoothing function with a 3% sampling portion.

the age model by 0.2 Ma toward younger ages (as can be supported by the $\delta^{18}O$ maximum at 14.2 Ma rather than 14.0 Ma, (Figure 3b) would align $\delta^{13}C$ maxima, albeit minor ones, with CM 3 and CM 4. CM 5 and CM 6 would be missing still as there are no variations in the $\delta^{13}C$ record near these events.

[35] Similarly to the other two sites, the paleoproductivity record does not show an overall trend during the middle

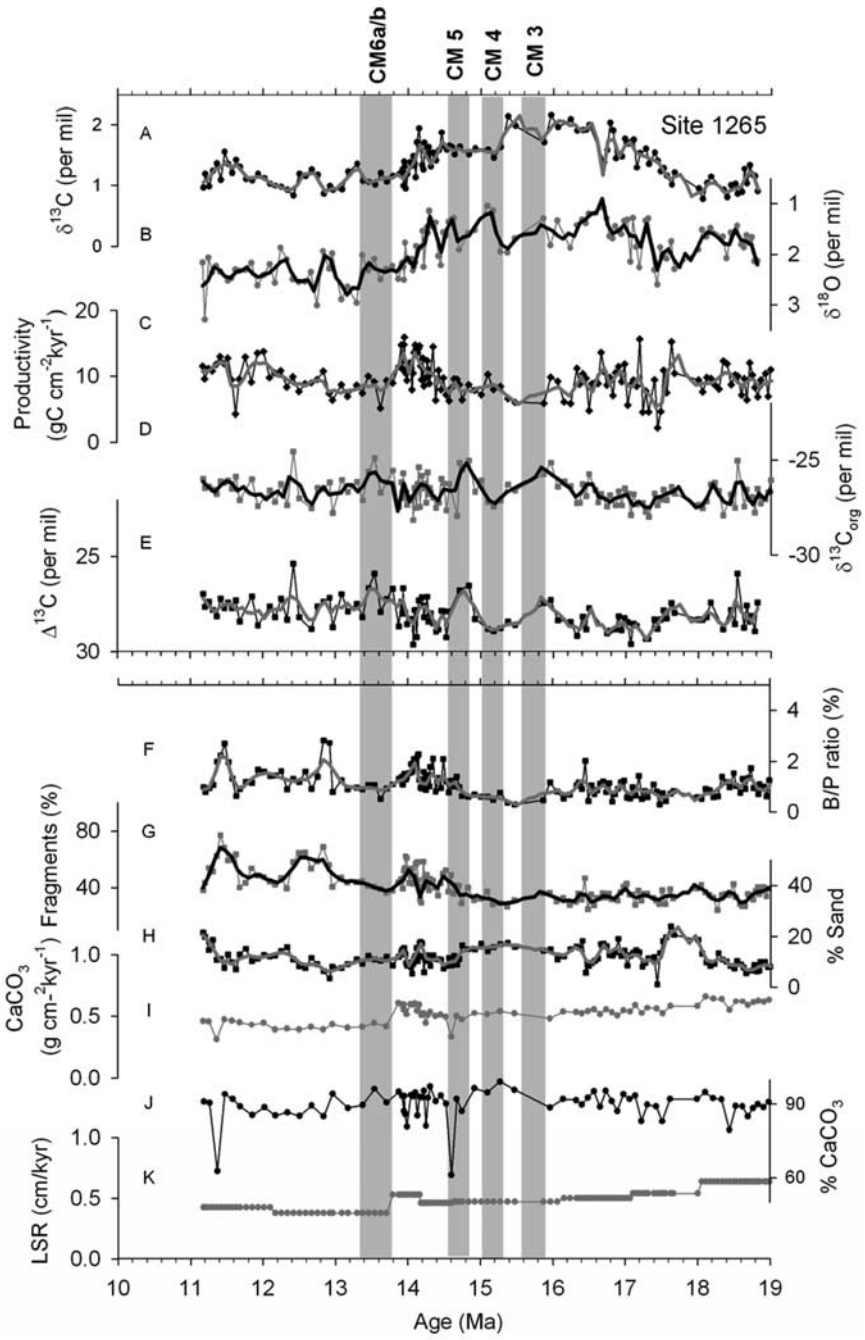

Figure 4. Results from South Atlantic Site 1265. (a) Benthic foraminiferal $\delta^{13}C$ values, (b) benthic foraminiferal $\delta^{18}O$ values, (c) benthic foraminiferal mass accumulation rate derived paleoproductivity, (d) $\delta^{13}C$ of bulk sedimentary organic matter ($\delta^{13}C_{org}$), (e) the difference between foraminiferal $\delta^{13}C$ values and $\delta^{13}C_{org}$, (f) percent benthic to planktonic (B/P) foraminferal test ratio, (g) percent fragments, (h) percent sand (>63 μm) fraction of the sediments, (i) $CaCO_3$ mass accumulation, (j) percent $CaCO_3$, and (k) linear sedimentation rates (LSR). Vertical gray bars highlight the position of Miocene carbon isotope (CM) events [*Woodruff and Savin*, 1991]. Heavy lines in Figures 4a–4h reflect a Gaussian smoothing function with a 3% sampling portion.

Miocene $\delta^{13}C$ maximum. The most notable feature in the paleoproductivity record at this site is a distinct maximum between ~14.5 and 14 Ma concurrent with increasing benthic foraminiferal $\delta^{18}O$ values and decreasing $\delta^{13}C$ values.

[36] Long-term trends in $\delta^{13}C_{org}$ are similar to the benthic foraminiferal $\delta^{13}C$ record with increasing values between ~17 and 16 Ma (Figure 4d). After 15.5 Ma when benthic foraminiferal $\delta^{13}C$ values decrease, $\delta^{13}C_{org}$ remains constant. As a result, the $\Delta\delta^{13}C$ curve is relatively invariant

until 15 Ma, and increases thereafter because of convergence of the two proxy records (Figure 4e). There is an interval of relatively high variability in the $\delta^{13}C_{org}$ record between ~14.5–14 Ma that corresponds to increased productivity, decreasing benthic foraminiferal $\delta^{13}C$ values, increasing $\delta^{18}O$ values, and hence to the major step in mid-Miocene Antarctic ice sheet growth.

[37] Linear sedimentation rates are very low (<1 cm ka^{-1}), and decrease further throughout the interval investigated (Figure 4k). There is a brief increase in LSR at ~14 Ma concurrent with the $\delta^{18}O$ maximum (Figure 4b). The material that does accumulate is almost exclusively $CaCO_3$ (Figure 4j). The percent fragments (Figure 4g) as well as the B/P ratio (Figure 4f) increase after 15 Ma when the percent sand fraction decreases (Figure 4h) suggesting increasingly more corrosive bottom waters. The effect of dissolution can also be seen in a slight decrease of the % $CaCO_3$ after 14 Ma (Figure 4j).

4.4. Elemental Ratios

[38] None of the three locations experienced an obvious enrichment of Ba or P_2O_5 over the detrital background (Figure 5). Ba concentrations are very low at Site 1265, but considerably higher at 608 and 925 (Figure 5a). This difference agrees with the generally low modern day productivity (Table 1) and apparently low Miocene paleoproductivity at Site 1265 (Figure 4c). Downcore, the Ba/Al_2O_3 ratios are inversely correlated to Al_2O_3 mass accumulation rates (not shown), a fact that excludes more detailed interpretation of Ba as a productivity proxy. Concentration of P_2O_5 is very low at all sites and there is no obvious enrichment over Al_2O_3 (Figure 5b). Consistent with Ba, lowest P_2O_5 concentrations are recorded at Site 1265 and agree with the comparatively nutrient poor environment in the modern and paleo-ocean. At all sites, the TiO_2 and Al_2O_3 weight percentages are linearly correlated (Figure 5c), reflecting a relatively constant sediment source at all sites; higher TiO_2 and Al_2O_3 concentrations at Site 925 as compared to the other sites underline the proximity of the Amazon River. The apparent lack of changes in nutrient or geochemical productivity proxies is consistent with the lack of long-term changes in paleoproductivity apparent in the other proxies.

[39] Auxiliary material is available electronically at World Data Center for Paleoclimatology, National Geophysical Data Center, NOAA, Boulder, Colorado, USA.[1]

5. Discussion

5.1. Benthic Foraminiferal $\delta^{13}C$ Records and Productivity

[40] In summary, the Atlantic sites do not show a change in benthic foraminifer-derived and geochemically derived paleoproductivity that would correspond to the overall, long-term maximum in the mid-Miocene benthic foraminiferal $\delta^{13}C$ records (Figure 6). The increase in productivity at Site 608 may be related to an age model–dependent increase in linear sedimentation rates, and it is thus ambiguous to what extent the pattern reflects the environmental signal. At Sites 608 and 925, individual $\delta^{13}C$ maxima superimposed on the long-term trend occur at the same time, reflect Miocene CM events, and suggest that the records have a consistent chronology. Decreasing the ages at Site 1265 by 0.2 Ma, as justified on the basis of the $\delta^{18}O$ record, would align individual $\delta^{13}C$ with CM 3 and CM 4, however the $\delta^{13}C$ maxima associated with CM 5 and CM 6 are missing. At this site, we observe a marked increase in productivity at 14 Ma, coincident with the decrease in $\delta^{13}C$ and increase in benthic foraminiferal $\delta^{18}O$ values reflecting Antarctic ice sheet expansion. We suggest that at Site 1265 the data may reflect the importance of regional processes on the $\delta^{13}C$ record and paleoproductivity.

[41] These data do not provide evidence for a link between the mid-Miocene $\delta^{13}C$ maximum and changes in marine primary productivity in the Atlantic Ocean. It may be that the long-term $\delta^{13}C$ trend of bottom waters is primarily controlled by processes operating on the global scale, while the individual productivity records reflect regional conditions that have little effect on bottom water $\delta^{13}C$ values. Our mid-Miocene time interval predates the evolution of Atlantic-Pacific $\delta^{13}C$ gradients associated with the formation of deep waters in the North Atlantic [*Wright et al.*, 1992; *Poore et al.*, 2006]. Thus, deep water circulation changes and associated variations in the $\delta^{13}C$ of benthic foraminifera cannot explain the observed relationship (or rather lack thereof).

[42] Our data also highlight that the beginning of the $\delta^{13}C$ excursion at about 17 Ma is not related to climatic changes, at least as recorded by the $\delta^{18}O$ values of benthic foraminifera, which do not indicate either a warming or a cooling at this time. This does not rule out that the end of the $\delta^{13}C$ shift is not linked in some way to the expansion of Antarctic ice at ~14 Ma. The $\delta^{13}C$ records return to preexcursion values at the end of the final of the CM events (CM 6) by about 13 Ma after cooling (i. e., the increase in $\delta^{18}O$ of benthic foraminifera) has reached a maximum. These observations attest to the complexity of the factors that can determine oceanic $\delta^{13}C$ values, which we further explore using a numerical model.

5.2. Bulk Sediment $\delta^{13}C$ Records and pCO_2

[43] In this study we have attempted to address the question whether atmospheric pCO_2 showed changes over this climate transition using the foraminiferal and bulk sedimentary organic matter $\delta^{13}C$ records. These paired records show broadly similar changes over the mid-Miocene, which implies that the positive $\delta^{13}C$ excursions during the mid-Miocene affected the entire oceanic carbon reservoir. This is particularly evident in the delta-delta ($\Delta^{13}C = \delta^{13}C_{carb} - \delta^{13}C_{org}$) curves (Figures 2e, 3e, and 4e), which are largely parallel and do not show any major shift in the isotopic fractionation between the carbonate and organic carbon reservoirs. Our data agree with Miocene pCO_2 reconstructions from haptophyte alkenone records [*Pagani et al.*, 1999, 2000; *Henderiks and Pagani*, 2007], boron isotopes and carbonate mineralogy [*Demicco et al.*, 2003] supporting that atmospheric CO_2 levels did not change significantly over the investigated interval of time.

[1] Auxiliary materials are available at http://www.ngdc.noaa.gov/paleo/index.html.

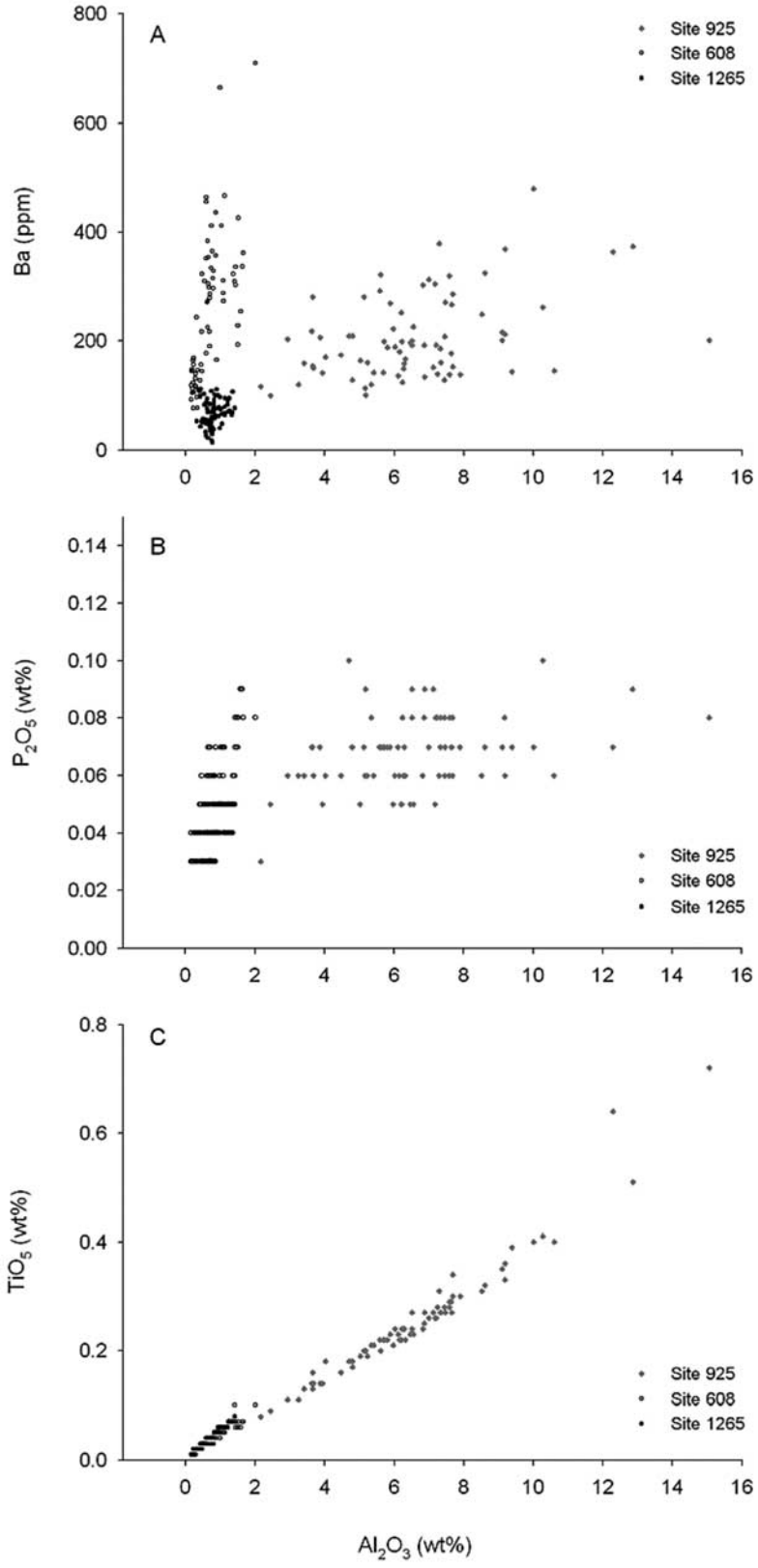

Figure 5. Scatterplots of (a) Ba (ppm), (b) P_2O_5 weight %, and (c) TiO_2 weight % as a function of Al_2O_3 weight % from Site 608 (open circles), Site 925 (gray diamonds), and Site 1265 (solid circles). All elemental ratios display linear trends that do not indicate any enrichment above terrigenous signals or changes in the terrestrial source regions.

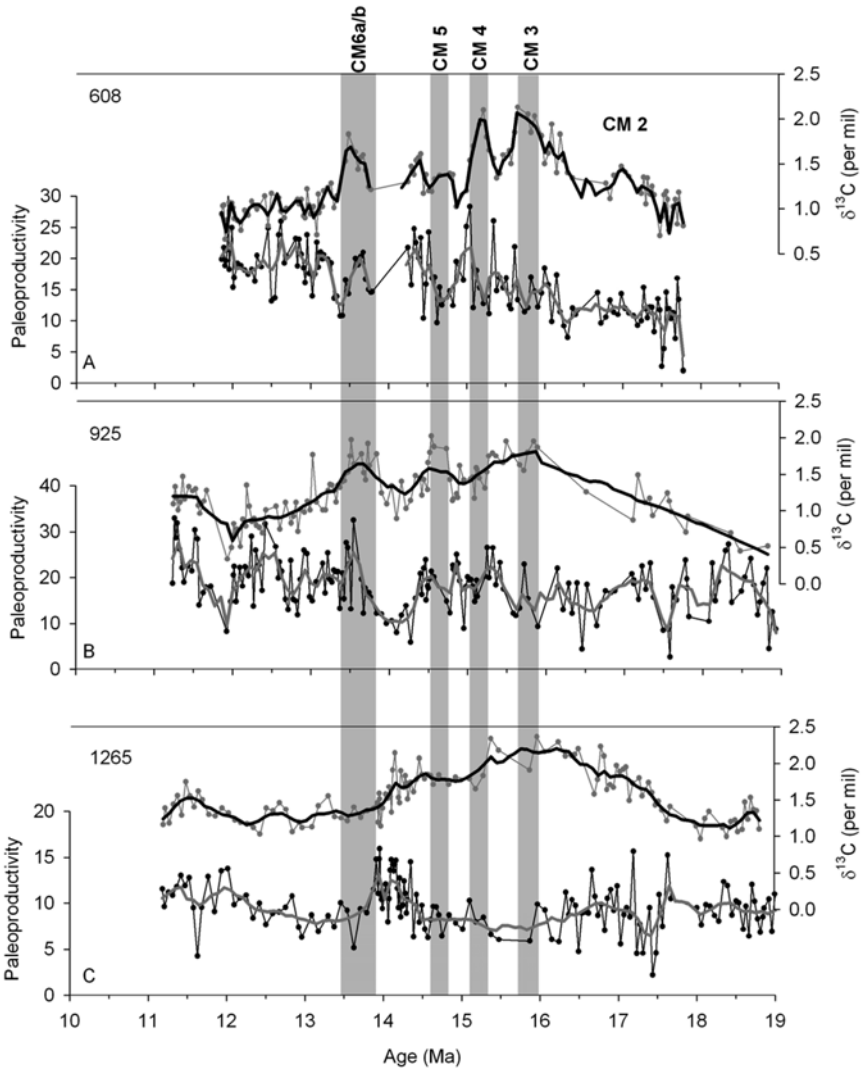

Figure 6. Synthesis of middle Miocene benthic foraminiferal δ^{13}C values and paleoproductivity records (units in gC cm^{-2} ka^{-1}). Vertical gray bars highlight the position of Miocene carbon isotope (CM) events [*Woodruff and Savin*, 1991]. Heavy lines reflect a Gaussian smoothing function with a 3% sampling portion.

The relatively high degree of background variability that is superimposed on the long-term average may reflect changing proportions of the type of organic matter being incorporated into the sediments, particularly at Site 925, where the decrease in $\delta^{13}C_{org}$ since 13.5 Ma may be related to increased supply of C_4 plant material from the early Amazon River [*Hoorn et al.*, 1995].

6. Numerical Sensitivity Tests

[44] We use a box-modeling approach to assess marine productivity, δ^{13}C records, and global carbon cycling. The aim of this modeling effort is to analyze the factors that may explain the positive δ^{13}C excursion of the deep ocean that occurred between 19 Ma and 13 Ma. Specifically, the isotopic effects of the following factors will be analyzed: (1) a warming of the surface ocean pool associated with the mid-Miocene climatic optimum; (2) possible changes in ocean productivity and/or organic carbon preservation in the water column or sediment, that may induce an increase in the marine organic carbon burial flux; and (3) enhanced deposition of organic carbon from the continents.

6.1. Surface Ocean Warming

[45] The global δ^{18}O curve [*Zachos et al.*, 2001], as well as continental paleovegetation data [e.g., *Mosbrugger et al.*, 2005], clearly mark the middle Miocene as a "climatic optimum." A potential rise of oceanic surface temperatures associated with generally warmer conditions may have altered the distribution of carbon isotopes among the carbonate species in the surface ocean [*Freeman and Hayes*, 1992] and hence the isotopic composition of the

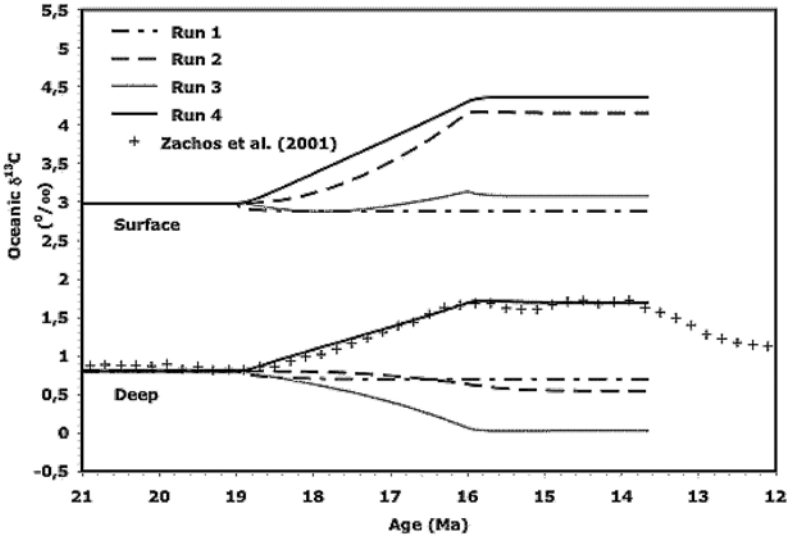

Figure 7. Variations of surface and deep ocean $\delta^{13}C$ in four different model scenarios starting from an early Miocene (19 Ma) preperturbation steady state. The deep ocean signal is compared to the data given by *Zachos et al.* [2001]. Run 1, step increase of ocean surface temperature by 2°C at 19 Ma; run 2, 50% (progressive) increase of ocean biological productivity between 19 and 16 Ma with constant organic carbon preservation in sediments; run 3, 50% (progressive) increase of ocean biological productivity between 19 and 16 Ma with reduced organic carbon preservation in sediments, so that organic carbon burial is kept constant; and run 4, continental organic matter deposition increases linearly from 2.3×10^{12} mol C a^{-1} to 3.3×10^{12} mol C a^{-1} between 19 and 16 Ma.

organic carbon and carbonate transferred to the deep sea or the sediment. Moreover, the warming can also be expected to affect the CO_2 solubility, which can modify the isotopic fractionation of marine organisms and, thus again, the isotopic composition of the transferred carbon. To test the influence of warmer surface temperature on the $\delta^{13}C$ of the deep ocean carbon reservoir, the surface ocean temperature in the model was increased abruptly by 2°C at 19 Ma. Note that this surface warming was not applied on the continents for the calculation of weathering rates, since continental temperatures are involved in the silicate weathering feedback and, thus, cannot be imposed externally in the model. Therefore, the change in continental temperatures may not be consistent with the change in ocean surface temperature in this sensitivity test, but the test should reveal the impact of the surface ocean warming on deep ocean $\delta^{13}C$ values. The results of this test are illustrated in Figure 7 (run 1) and show that surface ocean warming produces a decrease of the isotopic compositions of the surface and deep ocean carbon reservoirs by only 0.1‰, which is much smaller and of the opposite direction than the observed amplitude of the deep $\delta^{13}C$ excursion during the mid-Miocene climatic optimum. We rule out that an increase in sea surface temperatures affected the mid-Miocene deep ocean carbon isotopic excursion.

6.2. Marine Productivity and Organic Matter Preservation

[46] Although our proxy data do not indicate that marine productivity played a significant role in increasing the mid-Miocene carbon isotope values, we use the box model to numerically demonstrate that it is not possible to reproduce the isotope record by changing marine productivity (Figure 7, runs 2 and 3). We test the effect of a 50% progressive increase in global productivity over a 3 Ma long time interval. Primary productivity increase is artificially stimulated by increasing the input of phosphorus to the ocean. We conduct two simulations: In run 2 organic matter preservation is kept constant so that organic carbon burial increases in the ocean as productivity increases. In run 3, organic matter preservation is reduced in order to keep constant the oceanic organic carbon storage. In both runs, model productivity is increased from 2.5×10^{12} mol C a^{-1} to 3.77×10^{12} mol C a^{-1} (a 50% increase) keeping continental organic carbon deposition constant at its reference value of 2.3×10^{12} mol C a^{-1}. The results of these two experiments indicate that none produces the observed ~1‰ $\delta^{13}C$ increase in the deep ocean (Figure 7). In run 2 (constant organic matter preservation), the effect of the productivity increase is to enhance the $\delta^{13}C$ gradient between the surface and deep ocean. The $\delta^{13}C$ value of deep ocean decreases by 0.26‰, while the surface value increases by ~1‰. In run 3, (reduced organic matter preservation to keep organic carbon burial constant), we observe a large decrease (0.8‰) in the deep ocean, while surface isotopic $\delta^{13}C$ values remain constant (Figure 7).

[47] To assess the possible role of marine biology in the observed rise of the deep ocean $\delta^{13}C$ values, other combinations of ocean productivity and organic matter preservation (or organic carbon burial flux) than those illustrated in Figure 7 must be explored. As illustrated in Figure 8, several combinations of productivity and organic

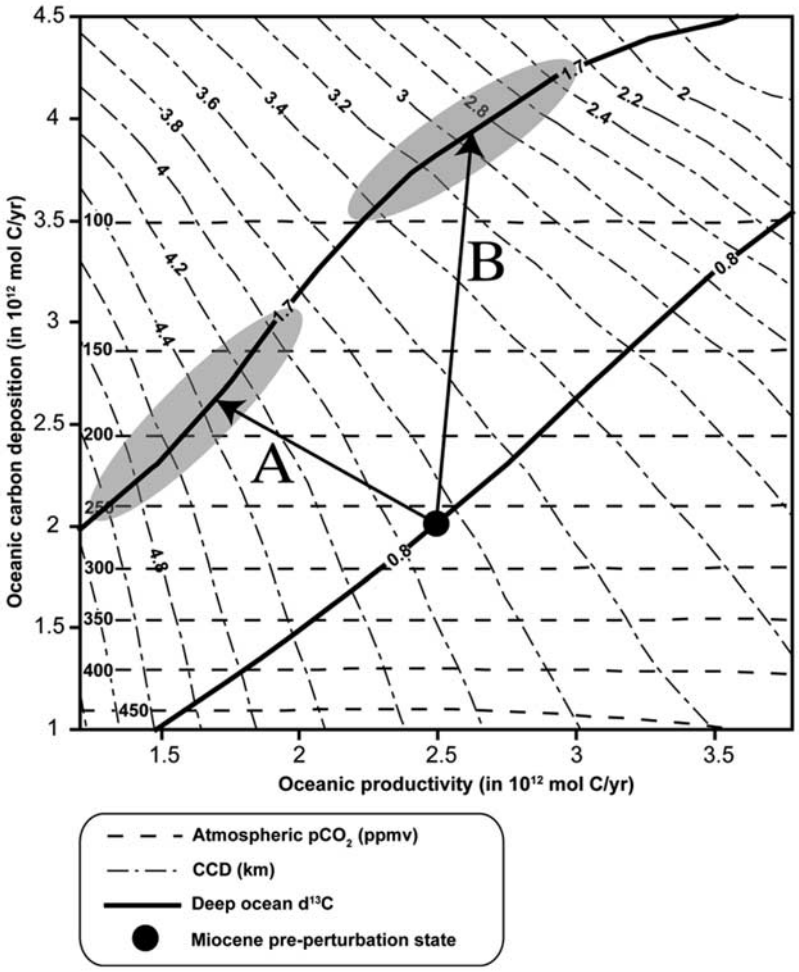

Figure 8. Model sensitivity to ocean productivity and/or ocean organic carbon deposition changes. The black circle represents the Miocene preperturbation state (19 Ma) from which the system evolves in response to a progressive change in productivity and/or organic carbon preservation over a 3 Ma time span (i.e., between 19 and 16 Ma). The isolines show the values of atmospheric CO_2 (pCO_2), calcite compensation depth (CCD), and deep ocean $\delta^{13}C$ in the steady state reached after the perturbation. The path followed by the model representative point must reach the 1.7‰ deep ocean $\delta^{13}C$ isoline (paths A and B) for the evolution to be consistent with the data given by *Zachos et al.* [2001].

carbon burial changes may lead to the observed change in $\delta^{13}C$ values. In Figure 8, the preperturbation state is represented by the black dot on the 0.8‰ deep ocean $\delta^{13}C$ isoline. This state corresponds to the 19 Ma preperturbation state in Figure 7. A perturbation in ocean productivity (x axis) and/or organic carbon burial (y axis) is applied over 3 million years to reach a new steady state at 16–14 Ma, similarly to the experiments shown in Figure 7. For the model to be consistent with *Zachos et al.*'s [2001] data, the model must reach the 1.7‰ deep ocean $\delta^{13}C$ isoline, following for instance arrows A or B. However, arrow A would result in a deepening of the model CCD, while data suggest a shallower CCD at 16 Ma by ~200–400 m [*van Andel*, 1975; *Opdyke and Wilkinson*, 1988] compared with the 19 Ma state. On the other hand, arrow B may be more consistent with the CCD change, but in this case atmospheric CO_2 reaches levels lower than 100 ppmv at 16 Ma, which is lower than pCO_2 reconstructions based on alkenone ^{13}C isotopic fractionation [*Pagani et al.*, 2000; *Henderiks and Pagani*, 2007, 2008], and boron isotopes [*Demicco et al.*, 2003]. Paths between arrows A and B are probably the most consistent with the data, although the decrease in atmospheric pCO_2 remains too large. However, possible reorganizations of surface to deep carbonate production/deposition (e.g., through an increase in coral reef formation or an increase of the aragonite:calcite ratio of carbonate productivity) between 19 and 16 Ma may result in a lowering of the CCD, so that path A may become more consistent with the data. Although such reorganizations are possible, we feel that path A (as well as intermediate A-B paths) remains unlikely, because our data indicate no change (at Sites 925, 1265) or possibly a slight regional increase in productivity (at Site 608). For these reasons we believe that any purely marine scenario is not a likely explanation for

the mid-Miocene positive excursion in deep ocean $\delta^{13}C$. Instead, the explanation for this excursion must be searched for on the continents.

6.3. Terrestrial Carbon Storage and pCO_{2atm}

[48] Enhanced organic carbon storage on land should result in an overall increase of the $\delta^{13}C$ of the Earth's surface system (including the ocean, the atmosphere and the terrestrial biosphere), and thus also the $\delta^{13}C$ values of the deep ocean. The importance of the response may depend on the magnitude of the atmospheric pCO_2 decrease, associated with the enhanced organic carbon sequestration, because ^{13}C fractionation of marine photosynthetic organisms is reduced at lower CO_2 levels. This fractionation effect is implemented in the model and results in a negative feedback, which tends to dampen the $\delta^{13}C$ fluctuation of the system.

[49] As illustrated in Figure 7 (run 4), the magnitude of the mid-Miocene positive excursion in deep ocean $\delta^{13}C$ records can be accounted for in our model by increasing linearly the organic C storage on land from the preperturbation value (2.3×10^{12} mol C a^{-1}) to 3.3×10^{12} mol C a^{-1} over a period of 3 Ma, which corresponds to an additional accumulation of 1.5×10^{18} mol C. Oceanic organic carbon burial and productivity remain constant. This continental carbon sequestration leads to an increase of the deep ocean $\delta^{13}C$ from 0.8‰ to 1.7‰ (Figure 7, run 4), which agrees with the global $\delta^{13}C$ record [*Zachos et al.*, 2001]. This imposed additional sequestration leads to a decrease in atmospheric pCO_2 from 264 ppmv to 135 ppmv, which is lower by ~50 ppmv than the minimum suggested by proxy reconstructions [*Henderiks and Pagani*, 2007]. Proxy-based estimates more in line with the model results are the minimum of 176 ppmv at 16.2 Ma according to phytoplankton ^{13}C isotopic fractionation data of *Pagani et al.* [2000] (for this period, change in cell size does not alter significantly the pCO_2 estimates according to *Henderiks and Pagani* [2008]), and the minimum of 126 ppmv at 15 Ma and 101 ppmv at 14.7 Ma according to boron isotopic data of *Demicco et al.* [2003]. This modeled change is accompanied by a small upward shift (360 m) of the model calcite compensation depth (CCD), a trend which is fully consistent with *van Andel*'s [1975] data. We note that neither the alkenone based proxy reconstructions nor the model output support the CO_2 estimates derived from stomatal frequency data of *Kürschner et al.* [2008], who indicate a p CO_2 of 500 ppmv during the mid-Miocene climate optimum.

[50] Our simulation thus supports the hypothesis of an increase in continental organic carbon sequestration. This terrestrial sink appears much more likely than any marine-based sink (see Figure 8), because the associated change in deep ocean $\delta^{13}C$ values and CCD are both consistent with the available data, while the modeled pCO_2 drop is significantly reduced with respect to the marine-based scenarios. Indeed, compared to the sequestration of marine organic carbon, the burial of terrestrial organic carbon has the advantage to limit the decrease in the atmospheric pCO_2 associated with the enhanced carbon sequestration, because terrestrial C_3 plants have significantly lower $\delta^{13}C$ signatures than marine organisms. The continental $\delta^{13}C$ signature may have even become more negative if, as can be expected, the continents became wetter during the mid-Miocene warming. In such a case, the amount of sequestered continental organic carbon required to explain the deep ocean isotopic shift would have been lower and so the decrease in atmospheric pCO_2 would also need to be smaller.

[51] It must be stressed that the CO_2 drop in the model is the direct consequence of the increased organic carbon deposition, which results from the constraint to follow the deep ocean $\delta^{13}C$ rise in the model. Hence, the rise of pCO_2 from ~300 ppmv at 20 Ma to almost 500 ppmv at 16 Ma suggested by the stomatal frequency data of *Kürschner et al.* [2008] is difficult to reconcile with the observed ~0.9‰ positive excursion during the same time interval of the deep ocean $\delta^{13}C$, which is a well-established variation of a carbon cycle proxy. Such an inconsistency of pCO_2 with a carbon cycle proxy is probably more difficult to resolve than the apparently small effect of pCO_2 on climate, which was invoked by earlier studies [*Pagani et al.*, 1999, 2000], as climate is affected by other forcing factors than CO_2 (other greenhouse gases, paleogeography and associated impacts of ocean circulation).

[52] It might be possible, however, to limit the model CO_2 drop associated with the deposition of organic carbon by two mechanisms. First, the calculated CO_2 change depends on the dependence on pCO_2 of the ^{13}C fractionation of marine (and terrestrial) photosynthesis adopted in the model. The slope of this relationship is not well known, while it may significantly affect the magnitude of the CO_2 drop. Second, our model assumes that CO_2 emission from volcanism remained constant between 19 and 16 Ma. This is based on *Cogné and Humler*'s [2006] reconstruction of seafloor spreading rates, which show very small variations during this period. However, the volcanism associated with Columbia River Basalts (CRB) is not taken into account in this reconstruction, while *Kürschner et al.* [2008] invoke it as a possible explanation for the mid-Miocene rise in CO_2 reconstructed from their stomatal frequency data. Might such an additional release of CO_2 by volcanism counterbalance for the sink associated with organic deposition?

[53] As a final thought, we have tested the impact of CRB in our model (see Appendix A for model details). The results show an atmospheric CO_2 level raised by only 9 ppmv during the eruption phase compared to the reference simulation (run 4) without CRB. After the eruption, when the emission of CRB CO_2 has ceased, atmospheric CO_2 stabilizes at 134 ppmv, i.e., 1 ppmv below the reference simulation. Consequently, the overall impact of CRB appears to be quite small.

[54] In summary, our model indicates that the increase of deep ocean $\delta^{13}C$ between 19 and 16 Ma implies that some 1.5×10^{18} moles of organic carbon must have been sequestered from the ocean-atmosphere system during this time interval. The consequence is a drop in atmospheric pCO_2, which appears exaggerated with respect to the most recent CO_2 reconstructions from geochemical data that suggest little change. An additional source of CO_2 with a ^{13}C isotopic signature close to (or above) that of the ocean, as for instance volcanism, is needed to reduce this atmospheric CO_2 drop and make the model more consistent

with the proxies. The amount of CO_2 emitted from CRB is too low to significantly reduce the pCO_2 drop, because of the small volume of basalts involved and to the fact that basalt weathering consumes at least part of the emitted CO_2. Therefore, it is continental organic carbon sequestration that can best explain the observed benthic foraminiferal $\delta^{13}C$ maximum, because (1) this is more consistent with the absence of any marked long-term trend in marine productivity evidenced by our data; (2) the ^{13}C fractionation of photosynthesis is larger in the terrestrial than in the marine realm, implying that the modeled atmospheric pCO_2 drop is lower and thus easier to reconcile with the CO_2 proxies; and (3) continental sequestration is consistent with the upward CCD shift observed in the ocean. We highlight that relatively large uncertainties surround the magnitude of the pCO_2 drop and the CCD shift, which depend on the kinetic rate constants (temperature and pCO_2 dependence) used for weathering, and the slope of the relationship between photosynthetic ^{13}C fractionation and pCO_2 used for the model inversion of the observed benthic foraminiferal $\delta^{13}C$ curve.

7. Summary and Conclusion

[55] We test if globally high benthic foraminiferal $\delta^{13}C$ values reflect enhanced sequestration of ^{12}C in pelagic sediments of the Atlantic Ocean during the period 17–14 Ma via an increase in marine productivity. Our results indicate that at all three sites examined, the long-term trend in geochemical- and foraminiferal-derived paleoproductivity does not follow the $\delta^{13}C$ record. Although the data from marine sediments do not indicate enhanced oceanic carbon sequestration in the mid-Miocene $\delta^{13}C$ maximum, we examine the amount of extra carbon stored and explore possible reasons for the shift with a numerical model. Sequestration of 1.5×10^{18} mol C over the period of 3 Ma leads to a 0.9‰ $\delta^{13}C$ positive excursion in the deep ocean, which is the observed magnitude in records. Global temperature changes (both positive and negative) have negligible impact on the isotopic composition of the deep ocean carbon reservoir. A rise in global marine productivity has the potential to cause the enrichment, but our empirical data suggest that deep-sea sediments in the Atlantic Ocean registered no such rise in productivity. An increase in continental organic carbon sequestration appears to be the most feasible way to enrich the ocean's carbon pool with ^{13}C, and is consistent with coeval lignite deposits worldwide.

Appendix A

A1. Model Description

[56] The model used here is a global geochemical box model including carbon, alkalinity and phosphorous cycle coupled with a one-dimension climate model. This later module is an energy balance model (EBM) that calculates the annual mean temperature in 18 latitudinal bands as a function of atmospheric pCO_2 [*François and Walker*, 1992]. The geochemical model is an updated version of the one used by *Grard et al.* [2005]. It contains an atmospheric box and 4 oceanic reservoirs: equatorial surface, polar surface, thermocline and deep layer (see Figure A1). Other modifications were performed, notably for the weathering laws that include a dependence on soil CO_2 and physical erosion (equations (A1)–(A3)).

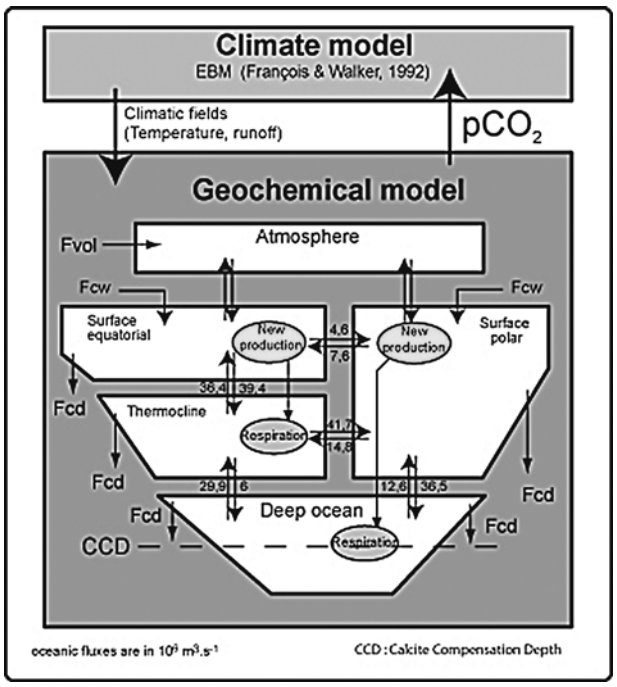

Figure A1. Structure of the box geochemical model used in this study.

$$f_{silw,i} = A_{sil,i} \cdot R_i \cdot \alpha \cdot \exp(C_{sil} \cdot WT) \cdot r_{co2} \cdot \sigma_{mech} \quad \text{(A1)}$$

$$f_{carw,i} = A_{car,i} \cdot \beta \cdot C_{car} \cdot Ca_i \quad \text{(A2)}$$

$$f_{orgw,i} = A_{org} \cdot R_i \cdot \gamma \cdot \sigma^{p}_{mech} \quad \text{(A3)}$$

$A_{sil,i}$ represent the continental area of exposed granitic or basaltic surfaces in latitude band i, R_i the continental runoff in latitude band i, α is constant for granite or basalt and calibrated for the present-day state in order to have the actual values for the weathering fluxes calculated by *Gaillardet et al.* [1999], C_{sil} is a constant representing the temperature dependence of the weathering rate for basalt and granite. WT is the average air temperature in °C during the weathering season, and is parameterized as a function of the annual mean temperature calculated by the EBM in each latitude bands [*Grard et al.*, 2005]:

$$\begin{aligned} &\text{if } T_i \le 252.16K \\ &WT = 0 \\ &\text{if } 252.16K < T_i 294.88K \\ &WT = 10.6783 + 0.508691 \cdot (T_i - 273.15) \\ &\text{if } T_i > 294.88K \\ &WT = T_i - 273.15 \end{aligned}$$

Table A1. Present-Day and Miocene Preperturbation (19 Ma) States of Some Model Fluxes and Parameters

Parameter	Present Day	Present-Day Flux $\delta^{13}C$	Miocene Preperturbation	Miocene Preperturbation Flux $\delta^{13}C$
f_{silw}	5.85×10^{12} mol a^{-1}	–	4.35×10^{12} mol a^{-1}	–
f_{carw}	12.3×10^{12} mol a^{-1}	3‰	12.13×10^{12} mol a^{-1}	3‰
f_{orgw}	4.5×10^{12} mol a^{-1}	−24.5‰	3.92×10^{12} mol a^{-1}	−24.5‰
f_{card}	18.15×10^{12} mol a^{-1}	1.68‰	16.43×10^{12} mol a^{-1}	2.45‰
f_{orgd}	2.0×10^{12} mol a^{-1}	−23.58‰	2.0×10^{12} mol a^{-1}	−22.52‰
f_{orgd_tb}	2.5×10^{12} mol a^{-1}	−25.18‰	2.3×10^{12} mol a^{-1}	−26.2‰
Atmospheric pCO_2	280.239 ppmv	−6.45‰	264.329 ppmv	−5.7‰
Deep ocean $\delta^{13}C$	0.15‰	–	0.799‰	–
Surface ocean $\delta^{13}C$	2.19‰	–	2.98‰	–

r_{co2} represents the concentration of soil pCO_2 relative to the present-day value, σ_{mech} is a global mechanical weathering factor normalized to 1 at present. The carbonate weathering law is a function of continental carbonate area (A_{car}), continental runoff (R_i) and calcium ion concentration in equilibrium with calcite and atmospheric CO_2 (Ca_i) in each latitude band.

[57] The kerogen weathering law is similar to the silicate weathering law, but no dependence on temperature is assumed and a power p is used for σ_{mech} (p = 0.3) [*Wallmann*, 2001].

[58] In the box model, a conservative equation is written for carbon (C_i), alkalinity (Alk_i), phosphorous (P_i) and carbon isotopic composition ($\delta^{13}C_i$) of each oceanic reservoir. The fluxes taken into account in these budgets involve both internal fluxes within the ocean atmosphere system (short-term fluxes) and external fluxes between this system and crustal reservoirs (long-term fluxes), (see Figure A1). The long-term fluxes are global mantle degassing (f_{vol}), carbonate deposition (f_{card}), organic carbon sequestration (f_{orgd}), continental carbonate weathering (f_{carw}) and continent organic-rich sediment weathering (F_{orgw}, kerogen weathering). The short-term fluxes are: mixing between ocean boxes (wmix), biological new production (Prod) and ocean-atmosphere CO_2 exchange.

A2. Model Calibration

[59] The model is calibrated on the present-day conditions in equilibrium with 280 ppmv. Carbonate and silicate weathering fluxes are calibrated to fit the present-day values proposed by *Gaillardet et al.* [1999]. The resulting, present-day values of all long-term carbon fluxes and $\delta^{13}C$ are presented in Table A1.

[60] The Miocene preperturbation state (19 Ma) is defined by applying Miocene paleogeography, by setting physical erosion to a value 35% lower than today [*Wold and Hay*, 1990] and by fixing global degassing to 4.73×10^{12} mol a^{-1}, a value derived from the change in seafloor accretion rate reported by *Cogné and Humler* [2006]. Oceanic organic carbon deposition is calibrated to a value of 2×10^{12} mol a^{-1} and continental organic carbon sequestration is fixed to 2.3×10^{12} mol a^{-1}. The model reaches a Miocene steady state with atmospheric pCO_2 at 264 ppmv, the calcite compensation depth (CCD) at 3875 m and the $\delta^{13}C$ of deep ocean at 0.799‰. These values for the Miocene (near 19 Ma) are in agreement with proxy data compiled by *Royer* [2006] for atmospheric pCO_2, with data from *van Andel* [1975] and *Opdyke and Wilkinson* [1988, 1993] for the CCD and with the data from *Zachos et al.* [2001], and this study, for the $\delta^{13}C$ of the deep ocean. The value of all long-term carbon fluxes and $\delta^{13}C$ for this preperturbation state are also listed in Table A1.

A3. Model Details Pertaining to the Columbia River Flood Basalts

[61] CRB and associated flood basalts of mid-Miocene age in North America have an estimated total volume of 234000 km^3 [*Hales et al.*, 2005], which corresponds to an emission of 1.24×10^{17} mol of CO_2, if the same ratio is assumed as for Deccan basalts [*Dessert et al.*, 2001]. Their eruption was initiated near 17 Ma and its main phase lasted approximately 1.3 Ma [*Hales et al.*, 2005; *Camp et al.*, 2003]. Total area of the CRB is 163700 km^2 [*Chesley and Ruiz*, 1998]. In the model, following the methodology used by *Dessert et al.* [2001] for the Deccan traps, we assumed that the CRB were emplaced between 17 Ma and 15.7 Ma, with a constant CO_2 emission flux of 9.54×10^{10} mol a^{-1} and a progressive linear increase of the basalt area over this time interval. This emplacement of CRB was implemented as a sensitivity test on run 4; that is, basalt emplacement occurs together with organic deposition on land.

[62] **Acknowledgments.** We are grateful to K. Föllmi, whose careful reading and constructive review have greatly improved this manuscript. We also thank an anonymous reviewer for suggestions and Eelco Rohling for handling the manuscript. Discussions with Ann Holbourn on the mid-Miocene are gratefully acknowledged. This research used samples provided by the Ocean Drilling Program (ODP). ODP is sponsored by the U.S. National Science Foundation (NSF) and participating countries under the management of the Joint Oceanographic Institutions (JOI) Inc. Funding for the organic carbon isotope analyses was provided by a Natural Sciences and Engineering Research Council (NSERC) discovery grant to D.R.G. (288321). We thank the Deutsche Forschungsgemeinschaft for financial support, as well as the Belgian National Foundation for Scientific Research (F.R.S.-FNRS; research grant 1.5.179.07, 2006–2007). L.D.H. thanks Jörn. Slotta and Johannes Schmidt at the University of the Saarland for preparing the bulk samples.

References

Anderson, R. F., and G. Winckler (2005), Problems with paleoproductivity proxies, *Paleoceanography*, *20*, PA3012, doi:10.1029/2004PA001107.

Antoine, D., J.-M. Andre, and A. Morel (1996), Oceanic primary production: 2. Estimation at global scale from satellite (coastal zone color scanner) chlorophyll, *Global Biogeochem. Cycles*, *10*, 57–69, doi:10.1029/95GB02832.

Averyt, K. B., and A. Paytan (2004), A comparison of multiple proxies for export production in the equatorial Pacific, *Paleoceanography*, *19*, PA4003, doi:10.1029/2004PA001005.

Berger, W. H., R. M. Leckie, T. R. Janecek, R. Stax, and T. Takayama (1993), Neogene carbonate sedimentation on Ontong Java Plateau: Highlights and open questions, *Proc. Ocean Drill. Program Sci. Results*, *130*, 711–744.

Billups, K., and D. P. Schrag (2002), Paleotemperatures and ice volume of the past 27 Myr revisited with paired Mg/Ca and $^{18}O/^{16}O$ measurements on benthic foraminifera, *Paleoceanography*, *17*(1), 1003, doi:10.1029/2000PA000567.

Browning, J. V., K. G. Miller, P. P. McLaughlin, M. A. Kominz, P. J. Sugarman, D. Monteverde, M. D. Feigenson, and J. C. Hernandez (2006), Quantification of the effects of eustasy, subsidence, and sediment supply on Miocene sequences, mid-Atlantic margin of the United States, *Geol. Soc. Am. Bull.*, *118*, 567–588, doi:10.1130/B25551.1.

Camp, V. E., M. E. Ross, and W. E. Hanson (2003), Genesis of flood basalts and basin and range volcanic rocks from Steens Mountain to the Malheur River Gorge, Oregon, *Geol. Soc. Am. Bull.*, *115*, 105–128, doi:10.1130/0016-7606(2003)115<0105:GOFBAB>2.0.CO;2.

Chesley, J. T., and J. Ruiz (1998), Crust-mantle interaction in large igneous provinces: Implications from the Re-Os isotope systematics of the Columbia River flood basalts, *Earth Planet. Sci. Lett.*, *154*, 1–11, doi:10.1016/S0012-821X(97)00176-3.

Cogné, J.-P., and E. Humler (2006), Trends and rhythms in global seafloor generation rate, *Geochem. Geophys. Geosyst.*, *7*, Q03011, doi:10.1029/2005GC001148.

Compton, J. S., S. W. Snyder, and D. A. Hodell (1990), Phosphogenesis and weathering of shelf sediments from the southeastern United States: Implications for Miocene $\delta^{13}C$ excursions and global cooling, *Geology*, *18*, 1227–1230, doi:10.1130/0091-7613(1990)018<1227:PAWOSS>2.3.CO;2.

Curry, W. B., et al. (1995), *Proceedings of the Ocean Drilling Program, Initial Results*, vol. 154, 1111 pp., Ocean Drill. Program, College Station, Tex.

Delaney, M. L., and E. A. Boyle (1987), Cd/Ca in late Miocene benthic foraminifera and changes in the global organic carbon budget, *Nature*, *330*, 156–159, doi:10.1038/330156a0.

Demicco, R. V., T. K. Lowenstein, and L. A. Hardie (2003), Atmospheric pCO_2 since 60Ma from records of seawater pH, calcium, and primary carbonate mineralogy, *Geology*, *31*, 793–796, doi:10.1130/G19727.1.

Derry, L. A., and C. France-Lanord (1996), Neogene growth of the sedimentary organic carbon reservoir, *Paleoceanography*, *11*, 267–275, doi:10.1029/95PA03839.

Dessert, C., B. Dupré, L. M. François, J. Schott, J. Gaillardet, G. J. Chakrapani, and S. Bajpai (2001), Erosion of deccan traps determined by river geochemistry: Impact on the global climate and the $^{87}Sr/^{86}Sr$ ratio of seawater, *Earth Planet. Sci. Lett.*, *188*, 459–474, doi:10.1016/S0012-821X(01)00317-X.

Diester-Haass, L., and S. Nees (2004), Late Neogene history of paleoproductivity and ice rafting South of Tasmania, in *The Cenozoic Southern Ocean: Tectonics, Sedimentation, and Climate Change Between Australia and Antarctica*, *Geophys. Monogr. Ser.*, vol. 148, edited by N. F. Exon, J. P. Kennett, and M. J. Malone, pp. 253–272, doi:10.1029/148GM18, AGU, Washington, D. C.

Diester-Haass, L., P. A. Meyers, and T. Bickert (2004), Carbonate crash and biogenic bloom in the Late Miocene: Evidence from ODP Sites 1085, 1086 and 1087 in the Cape Basin, southeast Atlantic Ocean, *Paleoceanography*, *19*, PA1007, doi:10.1029/2003PA000933.

Diester-Haass, L., K. Billups, and K.-C. Emeis (2005), In search of the late Miocene–early Pliocene "biogenic bloom" in the Atlantic Ocean (Ocean Drilling Program Sites 982, 925, and 1088), *Paleoceanography*, *20*, PA4001, doi:10.1029/2005PA001139.

Diester-Haass, L., K. Billups, and K.-C. Emeis (2006), Late Miocene carbon isotope records and marine biological productivity: Was there a (dusty) link?, *Paleoceanography*, *21*, PA4216, doi:10.1029/2006PA001267.

Dittert, N., K.-H. Baumann, T. Bickert, R. Henrich, R. Huber, H. Kinkel, and H. Meggers (1999), Carbonate dissolution in the deep-sea: Methods, quantification and paleoceanographic application, in *Use of Proxies in Paleoceanography*, edited by G. Fischer and G. Wefer, pp. 255–284, Springer, New York.

Dymond, J., E. Suess, and M. Lyle (1992), Barium in deep sea sediment: A geochemical proxy for paleoproductivity, *Paleoceanography*, *7*, 163–181, doi:10.1029/92PA00181.

Eagle, M., A. Paytan, K. R. Arrigo, G. van Dijken, and R. Murray (2003), A comparison between excess barium and barite as indicators of carbon export, *Paleoceanography*, *18*(1), 1021, doi:10.1029/2002PA000793.

Filippelli, G. M. (1997), Intensification of the Asian monsoon and a chemical weathering event in the late Miocene-early Pliocene: Implications for late Neogene climate change, *Geology*, *25*, 27–30, doi:10.1130/0091-7613(1997)025<0027:IOTAMA>2.3.CO;2.

Filippelli, G. M., and M. L. Delaney (1995), Phosphorous geochemistry and accumulation rates in the eastern equatorial Pacific Ocean: Results from Leg 138, *Proc. Ocean Drill. Program Sci. Results*, *138*, 757–767.

Flower, B. P., and J. P. Kennett (1993), Middle Miocene ocean-climate transition: High resolution oxygen and carbon isotopic records from Deep Sea Drilling Project Site 588A, southwest Pacific, *Paleoceanography*, *8*, 811–843, doi:10.1029/93PA02196.

Flower, B. P., and J. P. Kennett (1994), The middle Miocene climatic transition: East Antarctic ice sheet development, deep ocean circulation and global carbon cycling, *Palaeogeogr. Palaeoclimatol. Palaeoecol.*, *108*, 537–555, doi:10.1016/0031-0182(94)90251-8.

Föllmi, K. B., C. Badertscher, E. de Kaenel, P. Stille, C. M. John, T. Adatte, and P. Steinmann (2005), Phosphogenesis and organic-carbon preservation in the Miocene Monterey Formation at Naples Beach, California: The Monterey hypothesis revisited, *Geol. Soc. Am. Bull.*, *117*, 589–619, doi:10.1130/B25524.1.

Föllmi, K. B., B. Gertsch, J.-P. Renevey, E. De Kaenel, and P. Stille (2008), Stratigraphy and sedimentology of phosphate rich sediments in Malta and southeastern Sicily (latest Oligocene to early Miocene), *Sedimentology*, *55*, 1029–1051, doi:10.1111/j.1365-3091.2007.00935.x.

François, L. M., and J. C. G. Walker (1992), Modelling the Phanerozoic carbon cycle and climate: Constraints from the $^{87}Sr/^{86}Sr$ isotopic ratio of seawater, *Am. J. Sci.*, *292*, 81–135.

Francois, R., M. A. Altabet, R. Goericke, D. C. McCorkle, C. Brunet, and A. Poisson (1993), Changes in the $\delta^{13}C$ of surface water particulate organic matter across the subtropical convergence in the SW Indian Ocean, *Global Biogeochem. Cycles*, *7*, 627–644, doi:10.1029/93GB01277.

Francois, R. S., S. Honjo, S. J. Manganini, and G. E. Ravizza (1995), Biogenic Ba fluxes to the deep sea: Implications for paleoproductivity reconstructions, *Global Biogeochem. Cycles*, *9*, 289–303, doi:10.1029/95GB00021.

Freeman, K. H., and J. M. Hayes (1992), Fractionation of carbon isotopes by phytoplankton and estimates of ancient CO_2 levels, *Global Biogeochem. Cycles*, *6*, 185–198, doi:10.1029/92GB00190.

Gaillardet, J., B. Dupré, P. Louvat, and C. J. Allègre (1999), Global silicate weathering and CO_2 consumption rates deduced from the chemistry of large rivers, *Chem. Geol.*, *159*, 3–30, doi:10.1016/S0009-2541(99)00031-5.

Gradstein, F., J. Ogg, and A. Smith (2004), *A Geologic Time Scale 2004*, 589 pp., Cambridge Univ. Press, Cambridge, U. K.

Grant, K. M., and G. R. Dickens (2002), Coupled productivity and carbon isotope records in the southwest Pacific Ocean during the late Miocene–early Pliocene biogenic bloom, *Palaeogeogr. Palaeoclimatol. Palaeoecol.*, *187*, 61–82, doi:10.1016/S0031-0182(02)00508-4.

Grard, A., L. M. François, C. Dessert, B. Dupré, and Y. Goddéris (2005), Basaltic volcanism and mass extinction at the Permo-Triassic boundary: Environmental impact and modeling of the global carbon cycle, *Earth Planet. Sci. Lett.*, *234*, 207–221, doi:10.1016/j.epsl.2005.02.027.

Hales, T. C., D. L. Abt, E. D. Humphreys, and J. J. Roering (2005), A lithospheric instability origin for Columbia River flood basalts and Wallowa Mountains uplift in northeast Oregon, *Nature*, *438*, 842–845, doi:10.1038/nature04313.

Hayes, J. M., B. N. Popp, R. Takagiku, and M. W. Johnson (1989), An isotopic study of biochemical relationships between carbonates and organic carbon in the Greenhorn Formation, *Geochim. Cosmochim. Acta*, *53*, 2961–2972, doi:10.1016/0016-7037(89)90172-5.

Henderiks, J., and M. Pagani (2007), Refining ancient carbon dioxide estimates: Significance of coccolithophore cell size for alkenone-based pCO_2 records, *Paleoceanography*, *22*, PA3202, doi:10.1029/2006PA001399.

Henderiks, J., and M. Pagani (2008), Coccolithophore cell size and the Paleogene decline in atmospheric CO_2, *Earth Planet. Sci. Lett.*, *269*, 576–583, doi:10.1016/j.epsl.2008.03.016.

Herguera, J. C. (2000), Last glacial paleoproductivity patterns in the eastern equatorial Pacific: Benthic foraminifera records, *Mar. Micropaleontol.*, *40*, 259–275, doi:10.1016/S0377-8398(00)00041-4.

Herguera, J. C., and W. A. Berger (1991), Paleoproductivity from benthic foraminifera abundance: Glacial to postglacial change in the west-equatorial Pacific, *Geology*, *19*, 1173–1176, doi:10.1130/0091-7613(1991)019<1173:PFBFAG>2.3.CO;2.

Holbourn, A., W. Kuhnt, J. A. Simo, and Q. Li (2004), Middle Miocene isotope stratigraphy and paleoceanographic evolution of the northwest and southwest Australian margins (Wombat Plateau and Great Australian Bight), *Palaeogeogr. Palaeoclimatol. Palaeoecol.*, *208*, 1–22, doi:10.1016/j.palaeo.2004.02.003.

Holbourn, A., W. Kuhnt, M. Schulz, and H. Erlenkeuser (2005), Impacts of orbital forcing and atmospheric carbon dioxide on Miocene ice-sheet expansion, *Nature*, *438*, 483–487, doi:10.1038/nature04123.

Holdgate, G. R., I. Cartwright, D. T. Blackburn, M. W. Wallace, S. J. Gallagher, B. E. Wagstaff, and L. Chung (2007), The Middle Miocene Yallourn coal seam—The last coal in Australia, *Int. J. Coal Geol.*, *70*, 95–115, doi:10.1016/j.coal.2006.01.007.

Hoorn, C., I. Guerrero, G. A. Sarmiento, and M. A. Lorente (1995), Andean tectonics as a cause for changes in drainage patterns in Miocene northern South America, *Geology*, *23*, 237–240, doi:10.1130/0091-7613(1995)023<0237:ATAACF>2.3.CO;2.

Isaacs, C. M. (2001), Depositional framework of the Monterey formation, California, in *The Monterey Formation: From Rocks to Molecules*, edited by C. M. Isaacs and K. Rullkötter, pp. 1–30, Columbia Univ. Press, New York.

Jacobs, E., H. Weissert, and G. Shields (1996), The Monterey event in the Mediterranean: A record from shelf sediments of Malta, *Paleoceanography*, *11*, 717–728, doi:10.1029/96PA02230.

Jasper, J. P., and J. M. Hayes (1994), Reconstruction of palaeoceanic pCO_2 levels from carbon isotopic compositions of sedimentary biogenic components, in *Carbon Cycling in the Glacial Ocean: Constraints on the Ocean's Role in Global Climate Change*, *NATO ASI Ser. I*, vol. 17, edited by R. Zahn et al., pp. 323–341, Springer, Berlin.

Jia, G., P. Peng, Q. Zhao, and Z. Jia (2003), Changes in terrestrial ecosystem since 30 Ma in east Asia: Stable isotope evidence from black carbon in the South China Sea, *Geology*, *31*, 1093–1096, doi:10.1130/G19992.1.

John, C. M., K. B. Follmi, M. Mutti, E. Kaenel, T. Adatte, P. Steinmann, and C. Badertscher (2002), Carbonaceous and phosphate-rich sediments of the Miocene Monterey Formation at El Capitan State Beach (California), *J. Sediment. Res.*, *72*, 252–267, doi:10.1306/080701720252.

Keigwin, L. D. (1976), Late Cenozoic planktonic foraminiferal biostratigraphy and paleoceanography of the Panama Basin, *Micropaleontology*, *22*, 419–422, doi:10.2307/1485173.

Keigwin, L. D. (1987), Toward a high resolution chronology for the latest Miocene paleoceanographic events, *Paleoceanography*, *2*, 639–660, doi:10.1029/PA002i006p00639.

Keigwin, L. D., and N. J. Shackleton (1980), Uppermost Miocene carbon isotope stratigraphy of a piston core in the equatorial Pacific, *Nature*, *284*, 613–614, doi:10.1038/284613a0.

Keller, G., and T. A. Barron (1983), Paleoclimatic implications of Miocene deep sea hiatuses, *Geol. Soc. Am. Bull.*, *94*, 590–613, doi:10.1130/0016-7606(1983)94<590:PIOMDH>2.0.CO;2.

Kürschner, W. M., Z. Kvacek, and D. L. Dilcher (2008), The impact of Miocene atmospheric carbon dioxide fluctuations on climate and the evolution of terrestrial ecosystems, *Proc. Natl. Acad. Sci. U. S. A.*, *105*, 449–453, doi:10.1073/pnas.0708588105.

Loutit, T. S. (1981), Late Miocene paleoclimatology: Subantarctic water mass, southwest Pacific, *Mar. Micropaleontol.*, *6*, 1–27, doi:10.1016/0377-8398(81)90010-4.

Miller, K. G., J. D. Wright, and R. G. Fairbanks (1991), Unlocking the ice house: Oligocene-Miocene oxygen isotopes, eustasy, and margin erosion, *J. Geophys. Res.*, *96*, 6829–6848, doi:10.1029/90JB02015.

Mosbrugger, V., T. Utescher, and D. L. Dilcher (2005), Cenozoic continental climatic evolution of central Europe, *Proc. Natl. Acad. Sci. U. S. A.*, *102*, 14,964–14,969, doi:10.1073/pnas.0505267102.

Murray, D. W., and L. C. Peterson (1997), Biogenic carbonate production and preservation changes between 5 and 10 Ma from the Ceara Rise, western equatorial Atlantic, *Proc. Ocean Drill. Program Sci. Results*, *154*, 375–388.

Mutti, M., A. W. Droxler, and A. D. Cunnigham (2005), Evolution of the northern Nicaragua Rise during the Oligocene-Miocene: Drowning by environmental factors, *Sediment. Geol.*, *175*, 237–258, doi:10.1016/j.sedgeo.2004.12.028.

Nees, S. (1997), Late Quaternary palaeoceanography of the Tasman Sea: The benthic foraminiferal view, *Palaeogeogr. Palaeoclimatol. Palaeoecol.*, *131*, 365–389, doi:10.1016/S0031-0182(97)00012-6.

Opdyke, B. N., and B. H. Wilkinson (1988), Surface area control of shallow cratonic to deep marine carbonate accumulation, *Paleoceanography*, *3*, 685–703, doi:10.1029/PA003i006p00685.

Opdyke, B. N., and B. H. Wilkinson (1993), Carbonate mineral saturation state and cratonic limestone accumulation, *Am. J. Sci.*, *293*, 217–234.

Pagani, M., M. A. Arthur, and K. H. Freeman (1999), Miocene evolution of atmospheric carbon dioxide, *Paleoceanography*, *14*, 273–292, doi:10.1029/1999PA900006.

Pagani, M., M. A. Arthur, and K. H. Freeman (2000), Variations in Miocene phytoplankton growth rates in the southwest Atlantic: Evidence for changes in ocean circulation, *Paleoceanography*, *15*(5), 486–496, doi:10.1029/1999PA000484.

Peterson, L. C., and L. Stramma (1991), Upper level circulation in the South Atlantic Ocean, *Prog. Oceanogr.*, *26*, 1–73, doi:10.1016/0079-6611(91)90006-8.

Poore, H. R., R. Samworth, N. J. White, S. M. Jones, and I. N. McCave (2006), Neogene overflow of Northern Component Water at the Greenland-Scotland Ridge, *Geochem. Geophys. Geosyst.*, *7*, Q06010, doi:10.1029/2005GC001085.

Rau, G. H., T. Takahashi, and D. J. Des Marais (1989), Latitudinal variations in plankton $\delta^{13}C$: Implications for CO_2 and productivity in past oceans, *Nature*, *341*, 516–518, doi:10.1038/341516a0.

Rau, G. H., U. Riebesell, and D. Wolf-Gladrow (1997), $[CO_2]_{aq}$-dependent photosynthetic $\delta^{13}C$ fractionation in the ocean: A model versus measurements, *Global Biogeochem. Cycles*, *11*, 267–278, doi:10.1029/97GB00328.

Ravelo, A. C., et al. (1997), Pliocene carbonate accumulation along the California margin, *Paleoceanography*, *12*, 729–741, doi:10.1029/97PA02525.

Reitz, A., K. Pfeifer, G. de Lange, and J. Klump (2004), Biogenic barium and the detrital Ba/Al ratio: A comparison of their direct and indirect determination, *Mar. Geol.*, *204*, 289–300, doi:10.1016/S0025-3227(04)00004-0.

Retallack, G. J. (2001), Cenozoic expansion of grasslands and climate cooling, *J. Geol.*, *109*, 407–426, doi:10.1086/320791.

Royer, D. L. (2006), CO_2 forced climate thresholds during the Phanerozoic, *Geochim. Cosmochim. Acta*, *70*, 5665–5675, doi:10.1016/j.gca.2005.11.031.

Ruddiman, W. F., et al. (1987), *Initial Reports, Deep Sea Drilling Project, Leg 94*, vol. 1, 613 pp., U.S. Govt. Print. Off., Washington, D. C.

Savin, S., L. Abel, E. Barrera, D. Hodell, G. Keller, J. P. Kennett, J. Killingley, M. Murphy, and E. Vincent (1985), The evolution of Miocene surface and near surface marine temperatures: Oxygen isotope evidence, in *The Miocene Ocean: Paleoceanography and Biogeography*, edited by J. P. Kennett, *Mem. Geol. Soc. Am.*, *163*, 49–82.

Schmiedl, G., and A. Mackensen (1997), Late Quaternary paleoproductivity and deep water circulation in the eastern South Atlantic Ocean: Evidence from benthic foraminifera, *Palaeogeogr. Palaeoclimatol. Palaeoecol.*, *130*, 43–80, doi:10.1016/S0031-0182(96)00137-X.

Schmitz, B. (1987), Barium, equatorial high productivity and the northward wandering of the Indian continent, *Paleoceanography*, *2*, 63–77, doi:10.1029/PA002i001p00063.

Shevenell, A. E., J. P. Kennett, and D. W. Lea (2004), Middle Miocene Southern Ocean cooling and Antarctic cryosphere expansion, *Science*, *305*, 1766–1770, doi:10.1126/science.1100061.

Shipboard Scientific Party (2004), Site 1265, *Proc. Ocean Drill. Program Initial Rep.*, *208*, 1–107.

Siesser, W. G. (1995), Paleoproductivity of the Indian Ocean during the Tertiary Period, *Global Planet. Change*, *11*, 71–88, doi:10.1016/0921-8181(95)00003-A.

Southam, J. R., and W. W. Hay (1981), Global sedimentary mass balance and sea level changes, in *The Sea*, edited by C. Emiliani, pp. 1617–1684, John Wiley, New York.

Spivack, A. J., C.-F. You, and H. J. Smith (1993), Foraminiferal boron isotope ratios as a proxy for surface ocean pH over the past 21 Myr, *Nature*, *363*, 149–151, doi:10.1038/363149a0.

Utescher, T., V. Mosbrugger, and A. Ashraff (2000), Terrestrial climate evolution in northwest Germany over the last 25 million years, *Palaios*, *15*, 430–449.

van Andel, T. H. (1975), Mesozoic/Cenozoic calcite compensation depth and the global distribution of calcareous sediments, *Earth Planet. Sci. Lett.*, *26*, 187–194, doi:10.1016/0012-821X(75)90086-2.

van der Zwaan, G. J., I. A. P. Duijnstee, M. den Bulk, S. R. Ernst, N. T. Jannink, and T. J. Kouwenhoven (1999), Benthic foraminifers: Proxies or problems? A review of paleoecological concepts, *Earth Sci. Rev.*, *46*, 213–236, doi:10.1016/S0012-8252(99)00011-2.

Vincent, E., and W. H. Berger (1985), Carbon dioxide and polar cooling in the Miocene: The Monterey hypothesis, in *The Carbon Cycle and Atmospheric CO_2: Natural Variations, Archean to Present*, *Geophys. Monogr. Ser.*, vol. 32, edited by E. T. Sundquist and W. S. Broecker, pp. 455–468, AGU, Washington, D. C.

Vincent, E., J. J. Killingly, and W. H. Berger (1980), The Magnetic Epoch 6 carbon isotope shift, a change in the ocean's $^{13}C/^{12}C$ ratio: 6.2 million years ago, *Mar. Micropaleontol.*, *6*, 182–203.

Wallmann, K. (2001), Controls on the Cretaceous and Cenozoic evolution of seawater composition, atmospheric CO_2 and climate, *Geochim. Cosmochim. Acta*, *65*, 3005–3025, doi:10.1016/S0016-7037(01)00638-X.

Weedon, G. P., and N. J. Shackleton (1997), Inorganic geochemical composition of Oligocene to Miocene sediments and productivity variations in the western equatorial Atlantic: Results from Sites 926 and 929, *Proc. Ocean Drill. Program Sci. Results*, *154*, 507–526.

Wold, C. N., and W. W. Hay (1990), Reconstructing ancient sediment fluxes, *Am. J. Sci.*, *290*, 1069–1089.

Woodruff, F., and S. M. Savin (1985), $\delta^{13}C$ values of Miocene Pacific benthic foraminifera: Correlation with sea-level and biological productivity, *Geology*, *13*, 119–122, doi:10.1130/0091-7613(1985)13<119:CVOMPB>2.0.CO;2.

Woodruff, F., and S. M. Savin (1989), Miocene deepwater oceanography, *Paleoceanography*, *4*, 87–140, doi:10.1029/PA004i001p00087.

Woodruff, F., and S. M. Savin (1991), Mid-Miocene isotope stratigraphy in the deep sea: High resolution correlations, paleoclimatic cycles, and sediment preservation, *Paleoceanography*, *6*, 755–806, doi:10.1029/91PA02561.

Wright, J. G., K. G. Miller, and R. G. Fairbanks (1992), Early and middle Miocene stable isotopes: Implications for deepwater circulation and climate, *Paleoceanography*, *7*, 357–389, doi:10.1029/92PA00760.

Yasuda, H. (1997), Late Miocene-Holocene paleoceanography of the western equatorial Atlantic: Evidence from deep-sea benthic foraminifera, *Proc. Ocean Drill. Program Sci. Results*, *154*, 395–432.

Zachos, J., M. Pagani, L. Sloan, E. Thomas, and K. Billups (2001), Trends, rhythms, and aberrations in global climate 65 Ma to present, *Science*, *292*, 686–693, doi:10.1126/science.1059412.

K. Billups, College of Marine and Earth Studies, University of Delaware, 700 Pilottown Road, Lewes, DE 19958, USA. (kbillups@udel.edu)

L. Diester-Haass, Zentrum für Umweltwissenschaften, Universität des Saarlandes, D-66041 Saarbrücken, Germany. (l.haass@mx.uni-saarland.de)

K. C. Emeis, Institut für Biogeochemie und Meereschemie, Universität Hamburg, Bundesstrasse 55, D-20146 Hamburg, Germany. (kay.emeis@zmaw.de)

L. François, Institut d'Astrophysique et de Géophysique, Université de Liège, Bat. B5c, 17 Allée du Six Août, B-4000 Liège, Belgium. (francois@astro.ulg.ac.be)

D. R. Gröcke, Department of Earth Sciences, Durham University, Science Laboratories, South Road, Durham DH1 3LE, UK. (d.r.grocke@durham.ac.uk)

V. Lefebvre, UMR Géosystèmes, UFR des Sciences de la Terre, Université des Sciences et Technologies de Lille, Cité Scientifique, Bât SN5, F-59655 Villeneuve d'Ascq, France. (vincent.lefebvre@ed.univ-lille1.fr)